

國立交通大學

電子工程學系電子研究所

碩士論文

奈米碳管與錳氧化物奈米複合物
超高電容器的製作與其特性之研究



Fabrication and Characterizations of
Carbon Nanotube and Manganese Oxide
Nanocomposite Supercapacitor

研究生：洪政漢

指導教授：曾俊元

中華民國九十九年七月

奈米碳管與錳氧化物奈米複合物
超高電容器的製作與其特性之研究

Fabrication and Characterizations of
Carbon Nanotube and Manganese Oxide
Nanocomposite Supercapacitor

研究生：洪政漢

Student: Jeng-Han Hung

指導教授：曾俊元

Advisor: Tseung-Yuen Tseng



A Thesis

Submitted to Department of Electronics Engineering
and Institute of Electronics

College of Electrical and Computer Engineering

National Chiao Tung University

in partial Fulfillment of the Requirements

for the Degree of Master

in Electronics Engineering

July 2009

Hsinchu, Taiwan, Republic of China

中華民國九十九年七月

奈米碳管與錳氧化物奈米複合物超高電容器的製作與其特性之研究

學生：洪政漢

指導教授：曾俊元 博士

國立交通大學

電子工程學系電子研究所

摘 要

本論文探討利用氫離子作為表面活性劑，藉由電鍍製程製備出高效能與高循環次數的超級電容。超級電容是一種具有高比電容值、高功率密度、快速充放電等特性的儲能元件，其中藉由表面氧化物的價數變化達到儲能效果的稱為法拉第電容。目前以電鍍法或溶膠凝膠法製作法拉第電容通常需要高分子的表面活性劑，由於高分子在法拉第電容屬於阻值較大的物質，使得法拉第電容在高功率操作時有著嚴重的衰減。

本實驗藉由氫離子取代有機高分子來作為氧化錳的表面活性劑，使得氧化錳與奈米碳管複合材料的表面帶有正電荷，利用電鍍的方式在陰極沉積氧化錳與奈米碳管，由於少了高分子的影響使得超級電容在高功率下的衰減有效的減少。另外，本實驗也藉由加熱製程去有效的提升超級電容的比電容值，並且有效改善了法拉第電容在高循環次數下嚴重衰減的情形。

Fabrication and Characterizations of Carbon Nanotube and Manganese Oxide nanocomposite supercapacitor

Student : Jeng-Han Hung

Adviser : Prof.Tseung-Yuen Tseng

Department of Electronics Engineering and Institute of Electronics

National Chiao Tung University


Abstract

In this thesis, a high electrochemical performance and stability supercapacitor was produced by electrophoretic deposition (EPD) method using H^+ ion as surfactant to ionize the surface of manganese oxide. Supercapacitors are an energy storage device with high specific capacitance, high power density, and quickly charge/discharge time. Psuedocapacitor is one classification of supercapacitors which stores charge by changing the oxidation state of transition metal oxide. At present, polymer, a high charge transfer resistant material, is required as surfactant in EPD or sol-gel process leading to deadly recession of specific capacitance at high power density operating.

We substitute H^+ ion for polymer as surfactant of manganese leading MnO_x/CNT coaxial composite material to be ionized with positive charge so that they can be deposited on the cathodic electrode by EPD method. The situation of capacitance degradation at high scanning rate is improved due to without polymer. Besides an annealing step is introduced to this experiment to enhance the specific capacitance and reduce the degradation of capacitance after a long cycling test.

誌 謝

在這兩年碩士生涯裡，我首先要感謝指導教授曾俊元老師悉心的指導，並且在實驗中給了我明確的方向與目標，實驗室中也提供了許多儀器設備，讓我能夠順利的進行實驗。也要感謝老師時常在 meeting 時教誨著我們實驗的態度與做人處事的道理，讓我學習到許多專業外的知識。再來要感謝洪崇榮與姚奕全兩位學長在本論文上的相助，有著你們平時給的指導與意見，時常不辭辛勞陪我討論與材料分析，我才能夠順利完成本論文。



謝謝林孟漢、王聖裕、吳明錡、李岱螢、黃竣揚、李盈賢、葉昱廷等學長在課業上的指導，黃泰源、蘭以煒兩位同學一起互相學習，還有聖和、宗翰、家瑋學弟們平時的玩樂。因為有大家的陪伴，讓我的碩士生涯更佳的精彩與完整。

最後我要感謝我的家人，謝謝我的父母長期不辭辛勞的工作，努力的栽培我，讓我可以沒有負擔的一直念書。謝謝我的姊姊一直引領著我成長。因為你們的付出與關懷，才能成就今日的我。

Contents

Chinese Abstract.....	i
English Abstract.....	ii
Acknowledgement.....	iii
Contents.....	iv
Table Captions.....	vii
Figure Captions.....	viii
Chapter 1 Introduction	1
1.1 Introduction to Supercapacitors.....	1
1.1.1 The Characteristic of Supercapacitors.....	2
1.1.2 The Classification of Supercapacitors.....	3
1.2 Supercapacitors Materials.....	5
1.2.1 Active Carbons.....	5
1.2.2 Transition Metal Oxides.....	6
1.3 The Processes of Supercapacitors.....	8
1.3.1 Chemical Vapor Deposition.....	8
1.3.2 Hydrothermal Method.....	9
1.3.3 Sol-gel Method.....	9
1.3.4 Electrophoretic Deposition Method.....	10
1.4 Electrochemical Characteristic Measurement.....	11
1.4.1 Electrolyte.....	11
1.4.2 Measurement Method.....	13

Chapter 2 Experiment Details	24
2.1 Experiment Process Flow.....	24
2.2 Current Collector Preparation.....	25
2.2.1 Carbon Nanotubes Purification.....	25
2.2.2 Nickel Acid Treatment.....	26
2.2.3 Carbon Nanotubes Electrophoretic Deposition.....	26
2.3 Active Material Synthesis.....	27
2.3.1 MnO _x nanopowder.....	27
2.3.2 MnO _x /CNT Composite.....	27
2.4 Supercapacitors Preparation.....	28
2.5 Measurements and Analyses.....	29
2.5.1 X-Ray Diffraction.....	29
2.5.2 Scanning Electron Microscope.....	29
2.5.3 Field Emission Transmission Electron Microscope.....	30
2.5.4 X-ray Photoelectron Spectroscopy.....	30
2.5.5 BET Analysis.....	31
2.5.6 Thermal Gravimetric Analysis.....	32
2.5.7 Electrochemical Properties Measurements.....	32
Chapter 3 Results and Discussion	37
3.1 Supercapacitors Fabrication.....	37
3.1.1 Current Collectors Fabrication.....	38
3.1.2 Electrophoretic Deposition of Active Material.....	39
3.2 Material Analyses of MnO _x Nanopowder and MnO _x /CNTs Composite.....	39
3.3 Electrochemical properties of MnO _x nanopowder and MnO _x /CNT composite.....	41
3.3.1 Cyclic Voltammerty Measurement.....	41

3.3.2 Stability Test.....	42
3.4 Different Deposition Time and Voltage of MnO _x /CNT composite.....	44
3.5 Thermal annealing of MnO _x /CNT composite.....	45
3.5.1 Cyclic Voltammerty Measurement.....	45
3.5.2 Material Analyses.....	46
3.5.3 Impedance Analysis.....	46
3.5.4 Stability Test.....	47
 Chapter 4 Conclusion	 70
 Reference	 72



Table Captions

Table 2-1	Synthesis of active material.....	34
Table 2-2	Details of Chemicals used in this experiment.....	34
Table 2-3	EPD parameters of all samples in this experiment.....	35
Table 3-1	BET specific surface area analysis.....	48
Table 3-2	The specific capacitances of three different structures.....	48
Table 3-3	Specific capacitance verses density of deposit by adjusting EPD time and voltage.....	49
Table 3-4	Specific capacitances of MnO _x /CNT composite in various EPD parameters.....	49
Table 3-5	Specific capacitances of MnO _x /CNT composite after annealed for 2 hours.....	50
Table 3-6	XPS analysis of Mn _{2p3/2}	51
Table 3-7	1mA constant current stability test of MnO _x /CNT composite electrodes after annealed for 2 hours.....	51

Figure Captions

Fig.1-1	Specific power against specific energy for various electrical energy devices.....	17
Fig.1-2	electrochemical capacitors a) schematic of a commercial spirally wound double layer capacitor. b) Assembled device. c) A small button cell.....	17
Fig.1-3	schematic of fuel cell with supercapacitor as the power source module for vehicle.....	18
Fig.1-4	schematic view of electric double layer.....	18
Fig.1-5	Capacitive behavior of pseudocapacitor is composed of a series redox reaction segment.....	19
Fig.1-6	The area of I-V curve proportional to the operation voltage window	19
Fig.1-7	HRTEM images of (a) CNT and (b) MnO _x /CNT nanocomposite (inset is SAED of MnO _x nanoparticles).....	20
Fig.1-8	(a)CV curves of the a-MnO _x /CNTs/Ni electrode. (b) Variation of specific capacitances of a-MnO _x /Ni and a-MnO _x /CNTs/Ni electrodes with CV scan rate.....	20
Fig.1-9	SEM images of MnO ₂ and CNT coaxial structure.....	21
Fig.1-10	CVs for EPD of MnO ₂ ceramic and CNT charged by sodium alginate (a) 2mV/s, (b) 5mV/s and (c) 10 mV/s.....	21
Fig.1-11	SC versus scan rate (a) with CNT (b) without CNT.....	22
Fig.1-12	The IR drop in galvanostatic measurement when polarization of current changing.....	22
Fig.1-13	(a)Nyquist graph and (b)equivalent circuit model of an ideal supercapacitors.....	23
Fig.2-1	Illustration of the experimental flow.....	35
Fig.2-2	Illustration of the current collector fabrication flow.....	36
Fig.2-3	Illustration of the electrochemical measurement system.....	36
Fig.3-1	TEM image of MnO _x nanoparticle.....	52
Fig.3-2	TEM image of MnO _x /CNT coaxial composite.....	52
Fig.3-3	Thermal gravimetric analysis for MnO _x /CNT composite.....	53
Fig.3-4	SEM image of MnO _x /CNT composite on Ni foil.....	53
Fig.3-5	SEM image of MnO _x on CNTs/Ni foil.....	54
Fig.3-6	SEM image of MnO _x on Ni foil.....	54
Fig. 3-7	The CV curves of MnO _x /CNTs composite on Ni foil.....	55
Fig. 3-8	The CV curves of MnO _x on CNTs/Ni foil.....	55

Fig. 3-9	The CV curves of MnO _x on Ni foil.....	56
Fig. 3-10	The CV curves of three different structures scanned at 100mV/s.....	56
Fig. 3-11	The specific capacitance of three different structures versus scanning rates.....	57
Fig.3-12	Stability test of three different structures.....	57
Fig.3-13	SEM image of MnO _x /CNTs composite on Ni foil after 6000 cycles	58
Fig.3-14	SEM image of MnO _x on CNTs/Ni foil after 3000 cycles.....	58
Fig.3-15	SEM image of MnO _x on Ni foil after 3000 cycles.....	59
Fig.3-16	Cross section image of (a)30V-20mins (b)30V-40mins (c)30V-60mins (d)40V-20mins (e)40V-40mins (f)40V-60mins by FIB.....	60
Fig.3-17	Specific capacitance of MnO _x /CNTs composite deposited at 30V...	61
Fig.3-18	Specific capacitance of MnO _x /CNTs composite deposited at 40V...	61
Fig.3-19	The maintenances of specific capacitance of MnO _x /CNTs composite electrodes at different scanning rates.....	62
Fig.3-20	The diagram of specific capacitance at 100mV/s verse the density of deposits.....	62
Fig.3-21	Specific capacitance at 100mV/s of MnO _x /CNTs composite deposited at 30V after thermal annealing for 2 hours.....	63
Fig.3-22	Specific capacitance at 100mV/s of MnO _x /CNTs composite deposited at 40V after thermal annealing for 2 hours.....	63
Fig.3-23	XRD of MnO _x /CNTs composite electrodes after thermal annealing	64
Fig.3-24	XPS of MnO _x /CNTs composite electrodes after thermal annealing	64
Fig.3-25	Impedance analysis of MnO _x /CNTs composite electrodes after thermal annealing.....	65
Fig.3-26	TEM image of 30V-20mins after 6000 cycles without thermal annealing.....	65
Fig.3-27	1mA constant current stability test of MnO _x /CNT composite electrodes without thermal annealing.....	66
Fig.3-28	1mA constant current stability test of MnO _x /CNT composite electrodes after 150°C for 2 hours.....	67
Fig.3-29	1mA constant current stability test of MnO _x /CNT composite electrodes after 200°C for 2 hours.....	68
Fig.3-30	1mA constant current stability test of MnO _x /CNT composite electrodes after 250°C for 2 hours.....	69

Chapter 1

Introduction

1.1 Introduction to Supercapacitors

In recent years energy storage devices have become more important because the electronics industry has been developed rapidly. A high capacity and small size energy storage devices are required in many applications — such as telecommunication devices, Uninterruptible Power Supply, portable electric product, and electric/hybrid vehicles. Batteries and capacitors, plenty in our life, are two kinds of conventional energy storage devices. Batteries can store large amount of energy in a small volume, but short lifetime and low power density which causes a long charge/discharge time have been problems with most type of them. On the contrary, capacitors have advantages of high power density and long lifetime but low energy density. In order to satisfy the requirements of technology in the present age, we need to develop high energy capacity, high power density and long lifetime energy storage devices.

Supercapacitors, similar to a regular capacitor in operation, are called electrochemical capacitors using electrochemical reaction on the material of electrodes to store energy. The characteristics of supercapacitors are between batteries and capacitors: The power density and lifetime of them are much higher than that of batteries and the energy density of them is higher than that

of capacitors. Supercapacitors are a potential device that has high storage density, high power density and long lifetime and they can be combined with or substituted for traditional storage devices in many applications. The relationship of these three kinds of energy storage devices is illustrated in Fig.1-1 ¹.

1.1.1 The Characteristic of Supercapacitors

Supercapacitors, as an energy storage device with high power density and high energy density^{2,3}, could be used in power source application such as flashlight of digital camera, starter device for fuel cell and power supply for electric vehicles during acceleration^{4,5}. The charge/discharge rate of supercapacitors(>1kW/g) is more about 1000 times than that of batteries and the energy density of them is more about 1000~10000 times than that of capacitors. Addition to these, supercapacitors are easily assembled with other electronic devices and they can be fabricated on flexible substrate (Fig.1-2) which make high density package possible ^{6,7}.

One of supercapacitors application is hybrid capacitors⁸, which combines a supercapacitor with a battery so that they can benefit from both the supercapacitors and the batteries' properties. With high power density of supercapacitors, the combination of batteries and supercapacitors as power supplier systems will extend the lifetime of batteries and exhibit excellent performance. Take electric vehicles for example, the batteries and the supercapacitors are parallel in power supplier system. Fig.1-3 presents a schematic of a hybrid system. Batteries provide energy for vehicles and charge the supercapacitors when normal driving. During acceleration, vehicles need a

high power which is supplied from supercapacitors protecting battery from a large current flowed. Power supplier systems with supercapacitors can provide vehicles sufficient power all the time and extend batteries' lifetime because the damage, caused by fast discharge in batteries when accelerating, is eliminated.

1.1.2 The Classification of Supercapacitors

According to energy storage mechanisms, supercapacitors can be divided into two different types. First is based on the electric double layers in high surface area materials such as active carbon or carbon nanotubes. Second are pseudocapacitors that have a faradic charge exchange reaction on the active materials of electrode.

I . Electric double layers capacitors

Electric double layer capacitors (EDLCs) are an electrochemical capacitor which can store much more energy than conventional capacitor and offer much higher power density than batteries'. The first patent of electric double layer capacitors was filed in 1957 by Becker ¹, who used carbon increasing surface area coated on metallic current collector in a sulfuric acid solution. The charge storage mechanism, as shown in Fig.1-4, is using reversible physical adsorption of ions in the electrolyte by electrostatics ^{9,10}. There is no any faradic reaction in charge/discharge process, so the lifetime of EDLCs is much longer than pseudocapacitors'. When applying a voltage on electrode, charges separate and accumulate on polarization at the electrode-electrolyte interface, forming Helmholtz layer and Gouy layer storing a large amount of charge. Helmholtz layer is a dense ions layer and Gouy is

diffusion layer whose concentration of ions decays from helmoholtz layer to electrolyte. These ions layers and electrode with opposite charge work as two parallel conductor in conventional capacitor. Therefore EDLCs have capacitive behaviors.

According to Helmholtz's description in 1853, the capacitance C can be written as following:

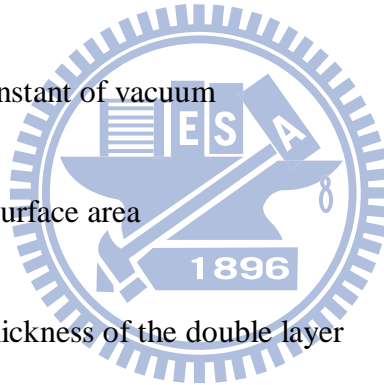
$$C = \frac{\epsilon_r \epsilon_0 A}{d} \quad [\text{Eq.1-1}]$$

ϵ_r : the electrolyte dielectric constant

ϵ_0 : the dielectric constant of vacuum

A : the electrode surface area

d : the effective thickness of the double layer



By equation [1-1], increasing the electrode surface area or decreasing the effective thickness of the double layer will increase the capacitance of EDLCs. But the effective thickness of the double layer in electrolyte is about several nanometers, it is arduous to reduce the effective thickness. Therefore using active carbon with high surface area or carbon nanotubes to extend the area of electrode has been researched in recently years.

II . Pseudocapacitors

The charge storage of pseudocapacitors is not only using electric double layer but also transferring ions of electrolyte to active material on electrode^{2,6,11}. That fast and reversible redox reactions occur at the surface of active materials allows pseudocapacitors to store more charges than EDLCs. Fig.1-5 shows that the charging /discharging behavior of pseudocapacitors is composed of a serial of redox reactions which are absorbing/desorbing ions on active materials. The I-V curve of pseudocapacitors is similar to conventional capacitors and the capacitance can remain a constant in different operation voltages as shown in Fig.1-6. But because redox reactions are used, pseudocapacitors, like batteries, often suffer from a lack of stability during cycling. So it has been a very important topic of how to extend the stability of pseudocapacitors and remaining their high capacitance in recently years.

1.2 Supercapacitors Materials

1.2.1 Active Carbons

Because the primary mechanism to store charges of EDLCs is physical ions absorption, the key to reaching high capacitance is using high specific surface area material with high conductivity as electrodes. There is a lot of material that could provide high surface area such like active carbon, fiber, carbon fabrics, templated and carbide-derived carbons, carbon nanotubes, onions and nanohorns carbon. Active carbons^{12,13}, like carbon black, are the most widely used material for EDLCs and because of their porous and high

surface area and moderate cost.

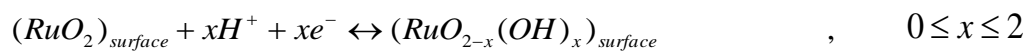
Carbon nanotubes are a potential material for EDLCs due to their high specific surface area and excellent conductivity¹⁴. Untreated carbon nanotubes have a lower capacitance than active carbon, but it can be increased by grafting oxygen rich groups which can help carbon nanotubes to absorb more ions from electrolyte¹⁵. Unfortunately, oxygenated groups are favorable to chemically react with protons, resulting in increasing series resistances and degeneration of capacitance.

1.2.2 Transition Metal Oxides

Pseudocapacitors use the fast redox reaction on the active material to store charges. Transition metal oxide is the most seen active material which have an unfilled d-space so that they can exhibit two or more oxidation states. A lot of transition metal oxides have been investigated for supercapacitors application such like CuO ¹⁶, Fe_2O_3 ¹⁷⁻¹⁹, Co_3O_4 ²⁰⁻²², NiO ²³⁻²⁵, RuO_2 ²⁶⁻²⁸, MnO_2 ²⁹⁻⁴⁰, V_2O_5 ⁴¹⁻⁴³ and etc. None of these oxides are used in commercial production and they are still in lab-scale research. The multi-state of oxidation allows a metal atom to store two or more charges. This is the reason why pseudocapacitors have a higher capacitance than EDLCs. If the metal oxide has a good crystalline structure, it is difficult for ions to diffuse into the inside of it. Because the effective metal oxide is limited to the surface, the inner oxide with high resistance causes cyclic voltammetry loop hysteresis, affecting the quality of charge/discharge behavior of supercapacitors. Amorphous metal oxide with hydrate has a thicker effective layer. Ions can be transferred from electrolyte into amorphous oxide much deeper than crystalline. Moreover, hydroxyl

groups in oxides are suitable sites for ions to insert, so that the capacitance can be raised⁴⁴⁻⁴⁶.

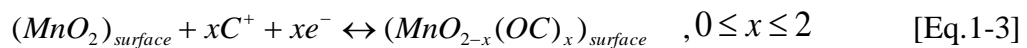
Ruthenium oxide, RuO₂, has been widely investigated in the past 40 years because it is conductive and has three distinct oxide states (II, III, IV) within 1.2 V, which is below the decomposed voltage of water^{26,27}. The reaction of charge storage can be presented as following:



[Eq.1-2]

RuO₂ has advantages of fast and reversible electron transfer with absorption of protons on the surface of it. Pataka reported that using electrophoretic method deposits a RuO₂ layer as a supercapacitor and the specific capacitance is as high as 650F/g²⁷. But ruthenium is too based expensive to be commercially attracted and the electrolyte of RuO₂-based supercapacitors is sulfuric acid which is dangerous for the environment.

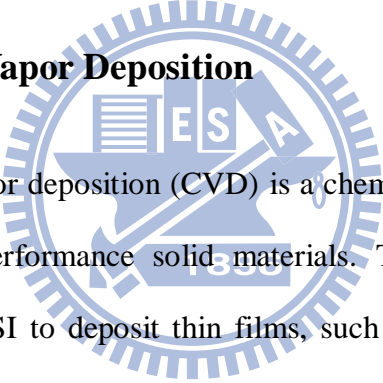
Manganese oxide, MnO₂, is a promising material because of low cost, high electrochemical activity and more friendly environmental nature than RuO₂. Manganese can be present in three different valence states and its oxides are highly complex. The storage mechanism is the insertion and extraction of protons or alkali metal cations such as Li⁺, Na⁺, and K⁺. The reactions can be written as following



Where $C^+ = H^+, Li^+, Na^+, \text{ and } K^{+47}$. According to theoretical calculation, the theoretical capacitance of manganese oxide reach to 1370F/g form Mn(II) to Mn(IV)³⁸; however, the conductivity of MnO₂ is a vital problem, because of the high resistance of bulk manganese oxide causing the capacitance in experiment behind the theorem. Lee reported that the capacitance can be enhanced to 418F/g by combining MnO₂ with CNTs to extend the surface area³³. This composite material, as shown in Fig.1-7, can increase the conductivity of electrode and the stability during cycling [Fig.1-8].

1.3 The Processes of Supercapacitors

1.3.1 Chemical Vapor Deposition



Chemical vapor deposition (CVD) is a chemical process used to produce high-purity, high-performance solid materials. This technique is extremely widely used in VLSI to deposit thin films, such as dielectric, semiconductor and metal layers. A number of forms of CVD are in widely use and are frequently referenced in the literature. These processes differ in the means by which chemical reactions are initiated and process conditions such as Atmospheric pressure CVD, Low Pressure CVD, Plasma Enhanced CVD, and etc. In a typical CVD process, precursor gases with high energy will be decomposed into radicals that diffuse into the surface of substrate and react to produce the desire and continuous deposit. Byproduct is also produced. It is very important that the byproduct must be gas so that they can diffuse back to the flow gas to be carried out. Otherwise byproduct remained on the substrate will reduce the quality of thin film. Reddy used CVD method and AAO

templates to successfully deposit high aligned coaxial MnO₂ and CNTs on Au electrode. The structure with high surface area allowing MnO₂ to trap more Li⁺ ions is shown in Fig.1-9³⁷.

1.3.2 Hydrothermal Method

Hydrothermal method utilizes chemical reaction in solution with different temperature and pressure in a sealed autoclave. Because the boil point of water can be changed by environment's pressure, the process temperature can be chosen above 100°C to 374°C by adjusting a appropriate pressure of autoclave. Hydrothermal synthesis has been an interesting method to produce materials with different nanoarchitectures such as nanorod, nanowires, nanoclakes, and etc. the advantage of hydrothermal method is the ability to control the nanostructure by properly choosing the temperature or time of the reaction or the active fill level in the pressure vessel or solvent used. Hashemzadeh and his co-workers reported that different crystalline phases and nanostructures of MnO₂ can be obtained by hydrothermal method in proper experimental parameters we discussed above⁴⁸.

1.3.3 Sol-gel Method

Sol-gel method is a simple process to fabricate the electrode of supercapacitors^{32,36,40}. The recipe of well-mixed active gel is about 80wt% nanopowder of MnO₂, 15wt% active carbon, and 5wt% binder, such as PTFE and PVDF, in organic solution. After coating the gel into metal electrode and burning the binder out by thermal annealing, the supercapacitor can be obtained. In the inner layer of active gel, binder which is a high resistance

material can't be burnt out completely, so there is a large IR drop during charge and discharge that reduces the performance of supercapacitors.

1.3.4 Electrophoretic Deposition Method

Electrophoretic deposition (EPD) is a process that uses electrical field to attract ions from solution to electrode where a faradic reaction takes place and deposit desired layer such as metals and oxides. The advantages of EPD are easy process, low cost for raw materials and equipment, fast deposition rate and safety when operating, therefore EPD has been widely researched for supercapacitors fabrication in recently years. The main technique modes in anodic deposition by EPD are potentiostatic²⁹, galvanostatic³⁰, and cyclic voltammetric method³¹. Ions with two positive charge such as Manganese Acetate ($\text{Mn}(\text{CH}_3\text{COO})_2$) and Manganese sulfate (MnSO_4) is the electrolyte for EPD process to deposit MnO_2 thin film. Because the grow rate of manganese oxide is varied in different plane direction, we can form many structure of manganese oxide like nanorods, nanoflakes, and nanoneedles by choosing different technique mode or combining them.

Because Electrophoretic deposition from ions is a fast reaction forming a thick and dense film, it is difficult to reach to high capacitance and maintain the stability. Deposition of ceramic by EPD is a possible solution to fabrication a high performance supercapacitors. However EPD of ceramic present difficult since it is hard to stable a well ceramic suspension. Particular surface charge is required for stability in suspension⁴⁹.

Zhitovskiy explored the phenomena that MnO_2 ceramic nanopowder and

CNTs absorbing some surfactants which are polymer such as sodium alginate³⁵, polyethylene³⁴, and dopamine³⁹ in solution can have positive charge in their surface so that they can deposit into electrode directly without any redox reaction by EPD method. This method provides a new way to fabricate supercapacitors that we can select and produce the desired structure and morphology of MnO₂ nanoparticles before deposited. The characteristics of cyclic voltammetry measurement and capacitance at different scanning rate are shown in Fig.1-10 and Fig.1-11. The result indicates that the capacitance decays deadly at high scanning rate because of the polymer surfactants that are a high charge transfer resistant substance. Therefore, we assume that finding a non-polymer and high conductive surfactant will improve the quality and stability of supercapacitors.

1.4 Electrochemical Characteristic Measurement

1.4.1 Electrolyte

The character of electrolyte when measuring is providing sufficient cations (H⁺, Li⁺, Na⁺, K⁺) for supercapacitors to store charge by fast redox reaction or electric double layer mechanism. In order to decrease the series resistance and improve the stability of supercapacitors, electrolyte must be not only high conductive but also stable to the package material of electrode. The radius of ions is a critical issue for supercapacitors. The smaller ions can diffuse quickly from electrolyte to the surface of electrode and penetrate to active oxide much deeper than large ions. Hydrogen ions provided from sulfuric acid or hydrochloric acid is the smaller cation using as electrolyte of

RuO₂, but considering its damage to environment, neutral solution is adopted for supercapacitors application.

The operation of supercapacitors is limited by the electrolyte decomposition at high voltage. That means the larger and stable electrolyte voltage window, the higher supercapacitor cell operating voltage. Since the energy density is proportional to the voltage squared (Eq.1-4.), it is necessary to develop and design high conducting, stable electrolyte with a wider voltage windows.

$$Energy = \frac{1}{2} CV^2 \quad [Eq.1-4]$$

To satisfy many applications in different operating voltage, the electrolyte can be divided into two types: aqueous and organic solution¹.

I . Aqueous Solution

Aqueous solution, such as H₂SO₄, KOH, Na₂SO₄, and KCl, has properties of high conductivity, high power density, low inner resistance. Using aqueous solution as electrolyte is convenience for supercapacitors and reduces the cost because the electrode doesn't need to dry and purify carefully during fabrication process of supercapacitors. But the decomposed voltage of water is 1.23V which limits the operation voltage of supercapacitors. Moreover, the application of supercapacitors in aqueous solution can be affected by temperature because increasing surrounding temperature will decrease the decomposed voltage of water, which is the upper limitation of voltage window⁵⁰.

II . Organic Solution

Supercapacitors benefit from organic solution with high operation voltage (2-3V) so that the storage energy is much higher than in aqueous electrolyte by Eq.1-4⁵¹. However the maximum power density in organic electrolyte is less than in aqueous because of poor conductivity which causes supercapacitors lager IR drop while charging and discharging. Organic solution is very sensitive to water. It is imperative for the process of supercapacitors to purify and dry strictly that ensures there is no water remained in electrode. The last but most important disadvantage of organic electrolyte is the price too expensive. The total cost of supercapacitor cell will be increased.

1.4.2 Measurement Method

The definition of capacitance is ratio of charge (Q) on the electrode to the operation voltage (V).

$$C = \frac{Q}{V}$$

[Eq.1-5]

In SI units, a capacitance of one farad means that one coulomb of charge on each conductor causes a voltage of one volt across the device. The lager capacitance stands for the lager ability to store charge. In supercapacitors we have to consider that how much capacitance can be contributed by one gram of active material. Therefore, Eq.1-5 is rewritten to Eq.1-6.

$$C = \frac{Q}{V \cdot g} \quad [\text{Eq.1-6}]$$

Where Q is storage charge, V is operation voltage window, g is the weight of active material and the unit of Q is gram.

There are two technical modes usually used to measure the performance of supercapacitors, and we will discuss all of these one by one as following.

I . Cyclic Voltammetry Method

Cyclic voltammetry measures the redox current of electrode within a given voltage range at a constant rate of voltage variation. Capacitance can be obtained by the following equation (Eq.1-7):

$$C = \frac{Q}{V \cdot g} = \frac{I \cdot t}{V \cdot g} \quad [\text{Eq.1-6}]$$

In this equation, symbol t, the charging or discharge time, can be calculated from scanning rate and operation voltage window. Integrating the redox current and time, we can get the number of storage charge and calculate specific capacitance.

Cyclic voltammetry is a useful method to estimate the electrochemical properties of electrode material of supercapacitors. It not only is used to calculate capacitance but also can identify the characteristic and adequate operation window for supercapacitors by the shape and the redox peak of cyclic voltammetry curve. Besides, whether the electrochemical reaction of

electrode is reversible or not can be referred to the symmetry of cyclic voltammetry and the charge/discharge area.

II . Galvanostatic Measurement

This method is using a constant current to charge and discharge supercapacitors in a given operation window. It is easy to know the amount of storage charge from the product of charge/discharge time and the current we choose. The reversibility of supercapacitors is easy to find out from the ratio of charge time to discharge and the symmetry of I-t curve. I-t curve also provide the magnitude of IR drop (Fig.1-12) that is contributed by internal resistance.

III . Impedance Measurement

Electrochemical impedance is usually measured by applying an AC potential to an electrochemical cell and measuring the current through the cell from high frequency to low frequency. According to Ohm's Law, dividing AC potential by AC current, we can know the magnitude of impedance Z and phase angle. These information are useful to analysis the interfaces resistance in measured cell and establish the equivalent circuit model.

The basic model of supercapacitors is a semicircle at high frequency and a 45° straight line at low frequency as shown in Fig.1-13. The first and second intercept on Z_{Re} axis denote electrolyte resistance R_{Ω} and charge transfer resistance R_{ct} respectively. At high frequency, the supercapacitor behavior is in kinetic control region because ac voltage signal is faster than surface reaction rate. When ac signal is near to surface reaction rate, we can find the charge

transfer resistance indicating that charge transferring from electrolyte to active material is easy or not. In low frequency region, the diffusible ability of cation is the dominated factor that means the charge transfer resistance is less than diffusion resistance in electrochemical system. We can use a constant phase element to describe diffusion control region. In an ideal supercapacitor, the phase of constant element is 45° is also called Warburg element σ assumed in semi-infinity diffusion model.



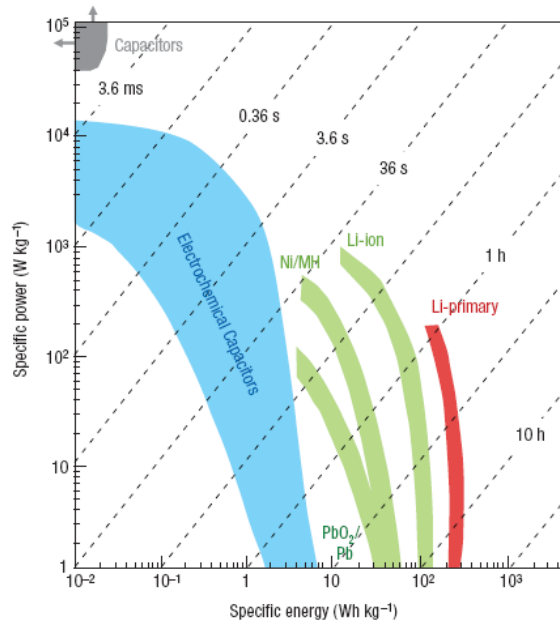


Fig.1-1 Specific power against specific energy for various electrical energy devices⁶

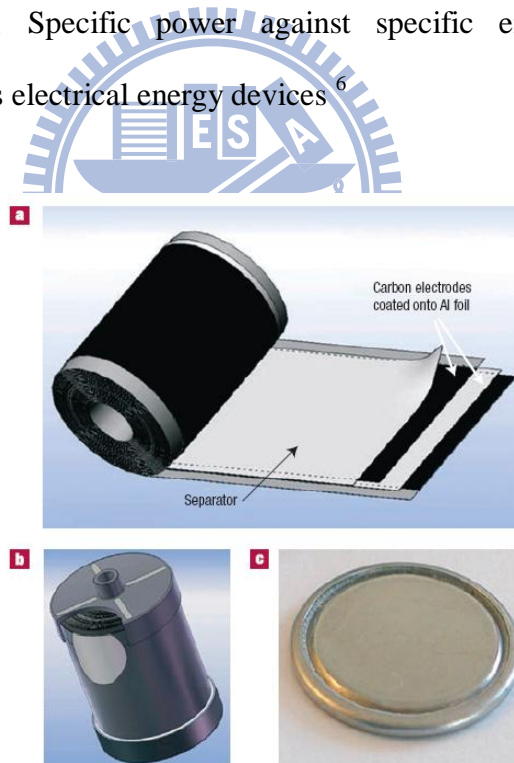


Fig.1-2 Electrochemical capacitors a) schematic of a commercial spirally wound double layer capacitor. b) Assembled device. c) A small button cell⁶

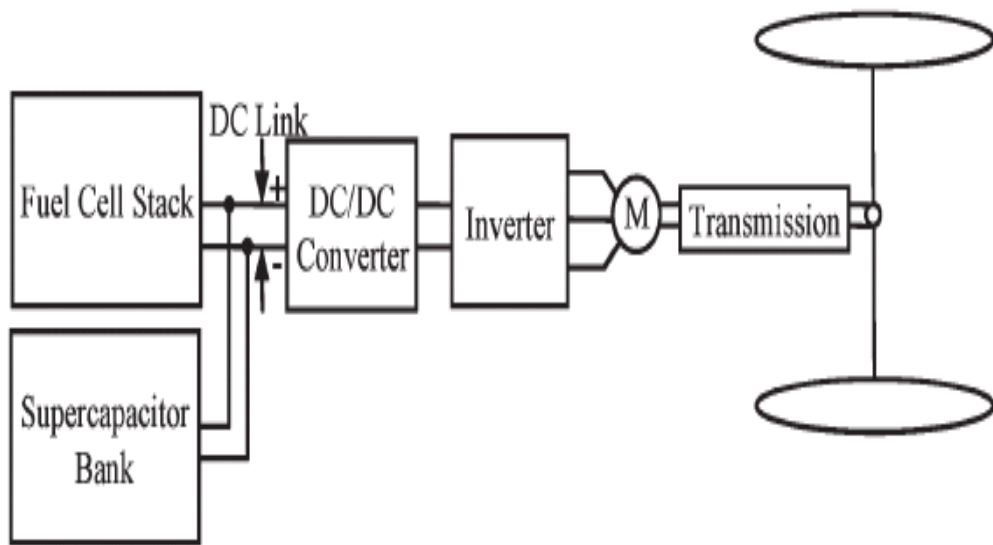


Fig.1-3 Schematic of fuel cell with supercapacitor as the power source module for vehicle⁴.

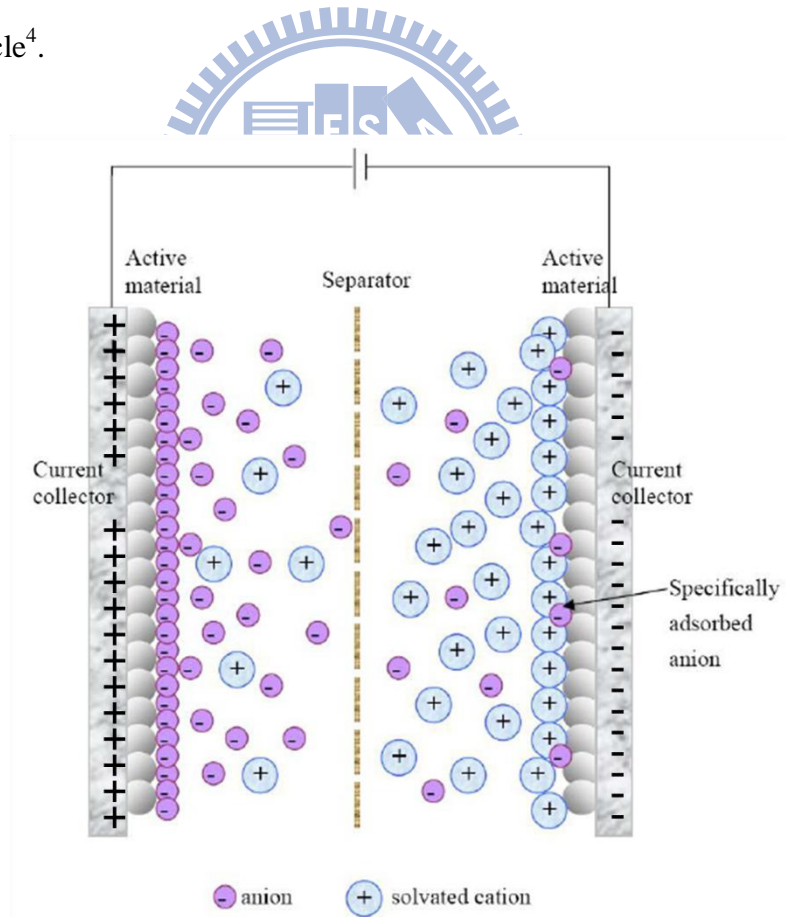


Fig.1-4 Schematic view of electric double layer

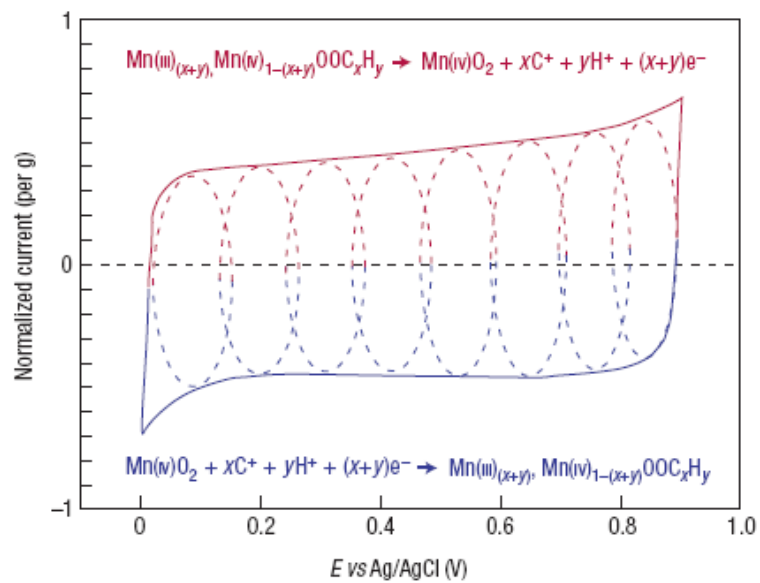


Fig.1-5 Capacitive behavior of pseudocapacitor is composed of a series redox reaction segment⁶.

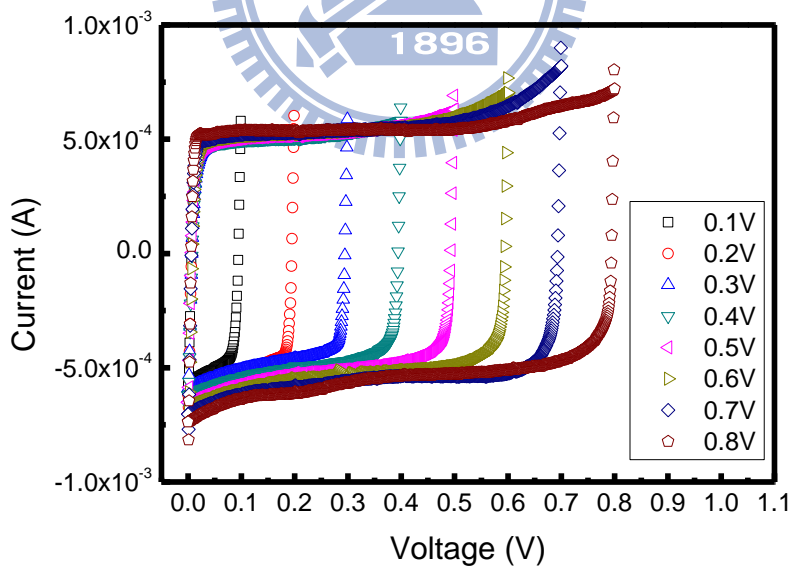


Fig.1-6 The area of I-V curve proportional to the operation voltage window

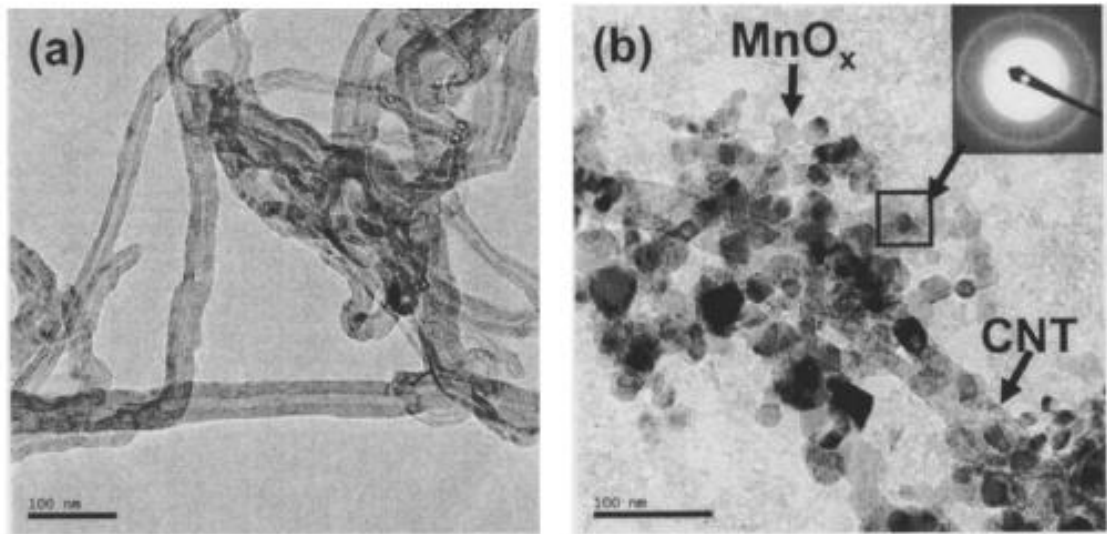


Fig.1-7 HRTEM images of (a) CNT and (b) MnO_x/CNT nanocomposite (inset is SAED of MnO_x nanoparticles)³³.

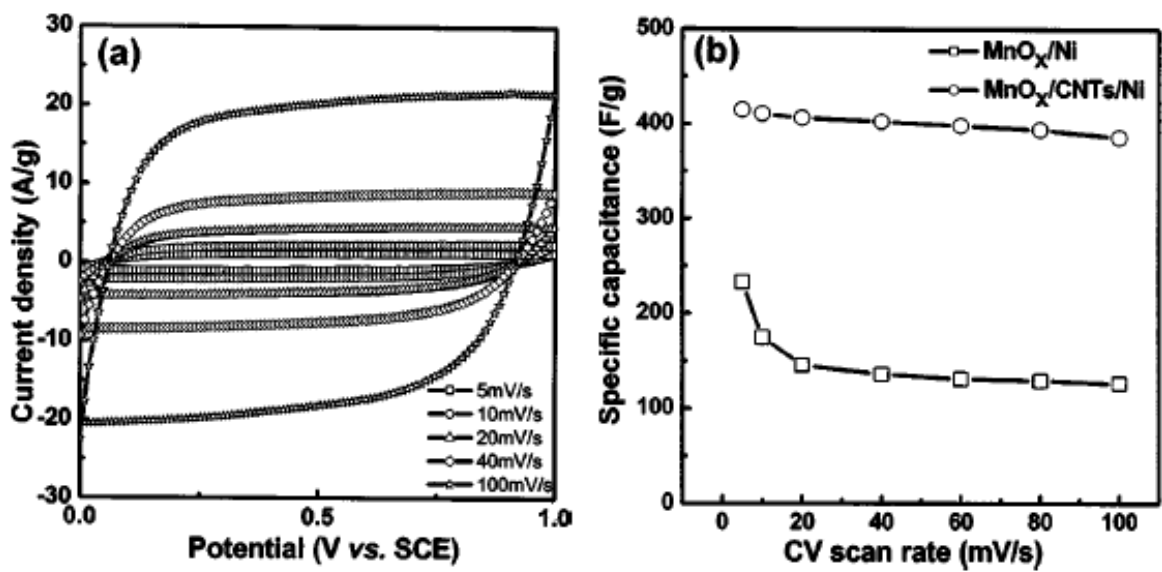


Fig.1-8 (a) CV curves of the a- $\text{MnO}_x/\text{CNTs}/\text{Ni}$ electrode. (b) Variation of specific capacitances of a- MnO_x/Ni and a- $\text{MnO}_x/\text{CNTs}/\text{Ni}$ electrodes with CV scan rate³³.

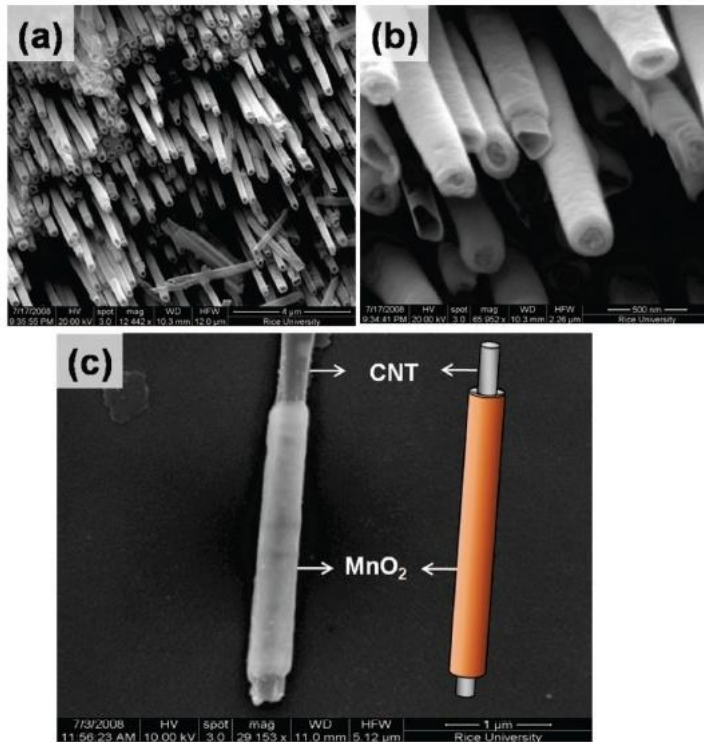


Fig.1-9 SEM images of MnO₂ and CNT coaxial structure.³⁷

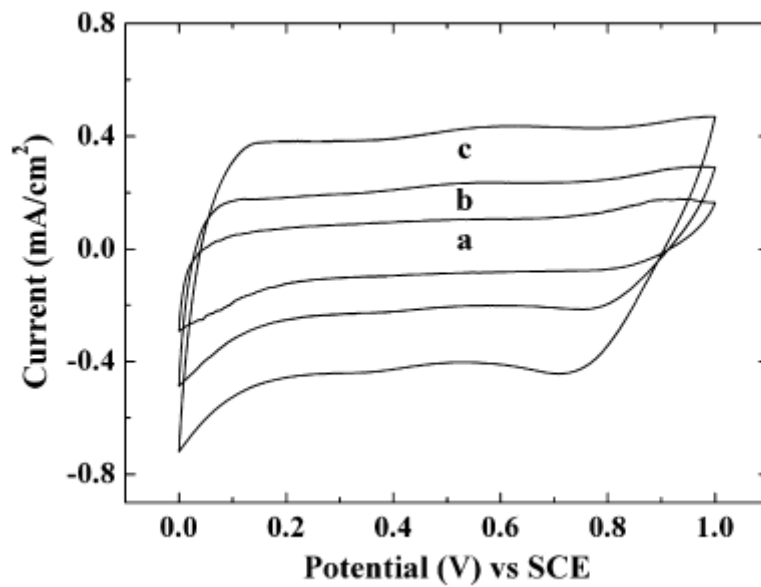


Fig.1-10 CVs for EPD of MnO₂ ceramic and CNT charged by sodium alginate (a) 2mV/s, (b) 5mV/s and (c) 10 mV/s³⁴.

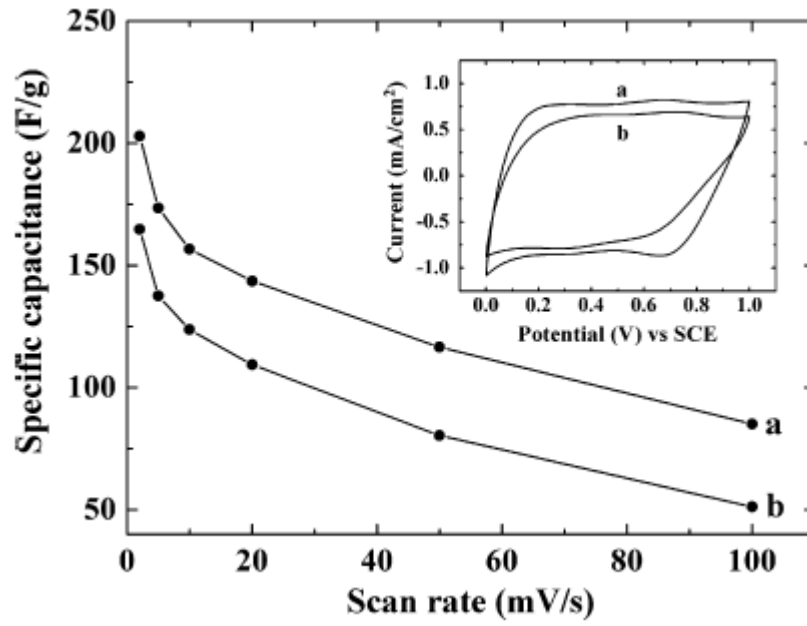


Fig.1-11 SC versus scan rate (a) with CNT (b) without CNT³⁴.

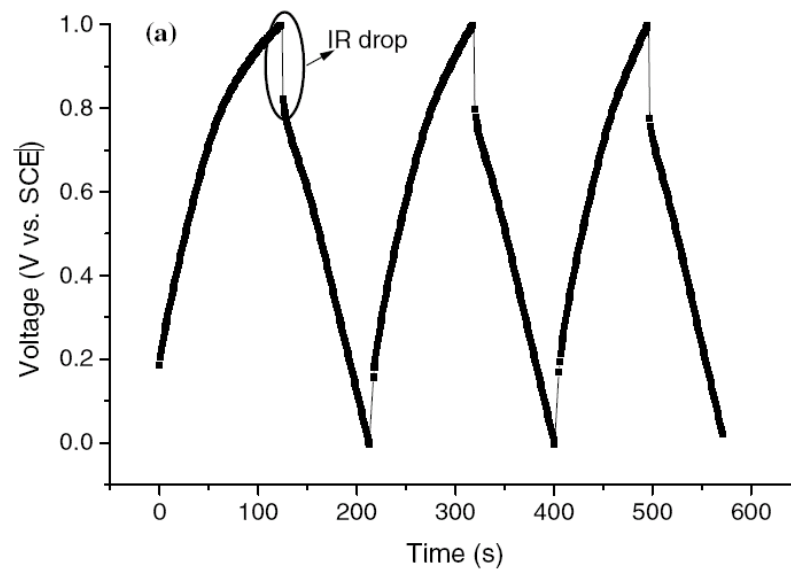


Fig.1-12 The IR drop in galvanostatic measurement when polarization of current changing⁵².

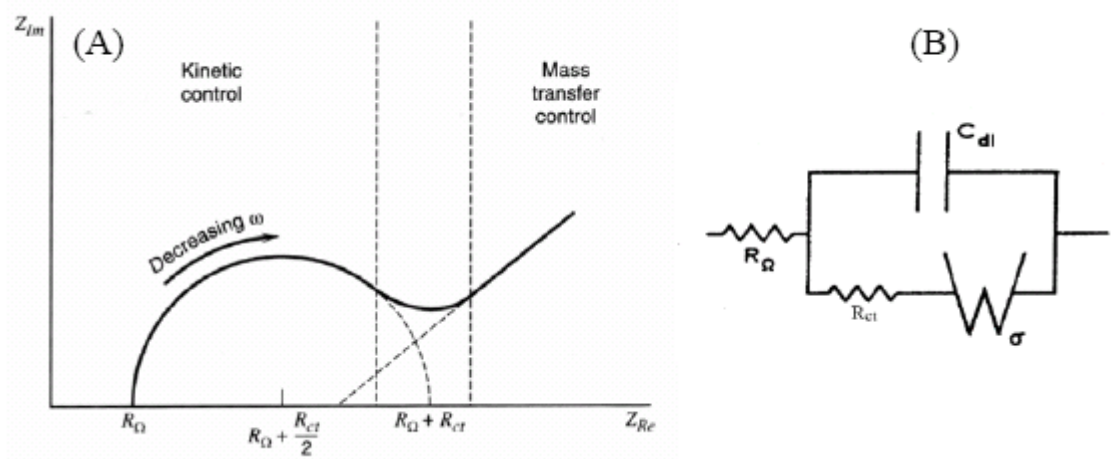
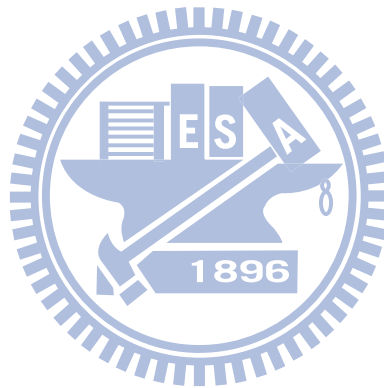


Fig.1-13 (a)Nyquist graph⁵³ and (b)equivalent circuit model⁵⁴ of an ideal supercapacitors.



Chapter 2

Experiment Details

2.1 Experiment Process Flow

The experiments are separated into two parts, including sample preparations and device characterizations analyses as shown in fig.2-1. There are several sample preparation steps described in this chapter.

First $1 \times 3 \text{ cm}^2$ Nickel foils with 1mm thickness as current collector were cleaned by ultrasonic agitation in ethanol for 10 minutes and their surface were roughed by a following nitride acid treatment. Three different device structures were fabricated in this thesis. Synthesis of MnO_2 powder and coaxial MnO_2/CNT were prepared before fabricating samples. Sample A used coaxial MnO_x/CNT composite material as the active layer, coated on nickel foil. Sample B was the MnO_x film coating on CNTs/Ni substrate which had been prepared previously. Sample C was the MnO_2 film coating on Nickel foils. All films were deposited by electrophoretic deposition method and all the samples needed to be dried in a oven at 80°C for 12 hours after every step. Considering the thermal effect on capacitive behavior, sample A was annealed by furnace for 2 hours. The details of experiment are described step by step in the following sections.

The scanning electron microscopy system (SEM) and X-ray diffraction system (XRD) were used to analyze surface morphology and the crystallization of the film, respectively. X-ray photoelectron spectroscopy (XPS) was used to measure the electronic state and empirical formula of MnO_x . Field emission transmission electron microscope (FETEM) was used to observe the structure of coaxial MnO_x/CNTs composite material. The components of composite material were analyzed by energy dispersive X-ray analyzer (EDX). BET and thermogravimetric analysis (TGA) were used to know the specific area of composite material and the ratio of MnO_x to CNTs, respectively. All the electrochemical performances of supercapacitors were measured by CH instruments 618B electrochemical analyzer.

2.2 Current Collector Preparation

2.2.1 Carbon Nanotubes Purification

Carbon nanotubes act as high surface current collector material on Nickel foil and the element of composite material. Before synthesis of MnO_x/CNTs material and depositing CNTs thin film, the CNTs need to be purified. The purification steps are following. First, 3.0 g multi-wall carbon nanotubes was added into 200ml 70% HNO_3 solution. This solution was stirred at 300rpm to keep MWCNTs well suspended and heated to boiling in reflux equipment for 24 hours. After cooled in the air, the purified MWCNT was washed to pH=7.0 by DI water and dried in an oven at 80°C for 12 hours.

2.2.2 Nickel Acid Treatment

The purpose for nickel acid treatment is to increase the surface roughness. 1x3 cm² polished nickel foils were cleaned by ultrasonic agitation in ethanol for 10 minutes. After that, eight pieces of the nickel foil was put in 200ml 10% diluted nitride acid and sonicated for 30 minutes. Then the nickel foils were washed by DI water and dried in an oven at 80°C for 12hours.

2.2.3 Carbon Nanotubes Electrophoretic Deposition

There are two kinds of current collector used in this thesis. One is the roughed nickel foil and another is the roughed nickel with CNTs thin film deposited by electrophoretic deposition method. The electrolyte of EPD contained 5mg purified CNTs and 5mg Mg(NO₃)₂ in 200ml isopropyl alcohol and dispersed well by ultrasonic agitation for 30 minutes. The Mg²⁺ ions acts as charge surfactant absorbed by oxygenated groups on CNTs surface so that the CNTs with positive charge on the their surface can be not only dispersed well in IPA but deposited in the cathode electrode⁵⁵. It is important for the quality of depositing CNTs film to use a well suspension as electrolyte.

Two roughed Ni foils were put in the suspension as cathode and anode electrodes. The space between two electrodes was 1 cm and the applied voltage of EPD was 40V for 30 minutes. Then the CNT/Ni substrate was put in an oven and dried at 80°C for 12 hours. The deposited area was restricted in 1x1cm². After that the CNTs/Ni current collector was fabricated completely.

2.3 Active Material Synthesis

In this thesis, manganese oxide is used for supercapacitors application. Two kinds of active material, as listed in table 2-1, MnO_x and MnO_x/CNT composite powder, were fabricated by chemical redox reaction.

2.3.1 MnO_x nanopowder

Potassium permanganate and Manganese sulfate were used as reductant and oxidant, respectively. 0.016M 90ml MnSO_4 solution was added into 0.005M 200ml KMnO_4 solution drop by drop in room temperature and stirred at 300rpm for 6 hours. Manganese oxide was precipitated from both of them. After washed to pH=7.0 by DI water and dried in an oven at 80°C for 12hours, MnO_x nanopowder was obtained.

2.3.2 MnO_x/CNT Composite

The process of the composite of MnO_x/CNT is similar to the MnO_x nanopowder. 0.4g purified MWCNTs was put in 0.005M 200ml KMnO_4 solution and dispersed by ultrasonic agitation for 30 minutes. Then adding 0.016M 90ml MnSO_4 into MWCNTs/ KMnO_4 solution drop by drop in room temperature and keeping the solution stirred at 300rpm for 6 hours will form the MnO_x/CNT composite powder. Finally, the powder was also washed to pH=7.0 by DI water and dried in an oven at 80°C for 12hours. The manufacturer and grade of chemicals used are listed in table 2-2.

2.4 Supercapacitors Preparation

The electrophoretic deposition (EPD) method was adopted to deposit the active material powder on current collector. The electrolyte of EPD was composed of 0.24g active powder and 0.4 ml 37% HCl in 4 l isopropyl alcohol and dispersed well by ultrasonic agitation for 30 minutes. Three kinds of current collector and nickel foil were put in the electrolyte as cathode and anode electrodes, respectively. The space between two electrodes was 1 cm.

The structure of sample A is MnO_x/CNT composite material coated on roughed Ni foil and the applied voltage of EPD was 30V and 40V for 20, 40 and 60 minutes. The current collectors of Sample B and Sample C were roughed CNTs/Ni and nickel substrate, respectively. MnO_x nanopowder was used as active material and deposited on the cathode at 30 V applied voltage for 20 minutes. The MnO_x and MnO_x/CNT composite material were also deposited on the cathode electrode. All the depositions were fixed in $1 \times 1 \text{cm}^2$ and needed drying in an oven at 80°C for 12hours. In order to know the thermal effect on capacitive behavior of MnO_x/CNT composite supercapacitors, sample C put in furnace was annealed to 150°C , 200°C , and 250°C in air for 2 hours, respectively. All experiment parameters of samples are shown in table 2-3.

2.5 Measurements and Analyses

2.5.1 X-Ray Diffraction (XRD)

Generally, thin films are classified according to its crystallization. There are three types of crystallization, including amorphous, polycrystalline, and crystalline. XRD analysis was used to investigate the crystal structure and orientation of our sample. Furthermore, the crystallization dependence of the samples could be identified for heat treatment. In the experiment, the thin films were grown between amorphous type and poly type. By Scherrer's formula, $D = \frac{0.9 \times \lambda}{B \times \cos \theta}$, this could estimate the average grain size from XRD illustration. Where the background information of the XRD analysis is that $\lambda = 1.5405 \text{ \AA}$ ($K\alpha$), B is the full width at half maximum (FWHM) of the XRD peak and θ is the diffraction angle. In this analysis, X-ray was made with 0.02 degree beam divergence and operation configuration at 30KV, 20mA.

2.5.2 Scanning Electron Microscope (SEM)

Comprehensively, the surface morphology issue is also a quite important character compared with the character of bulk for the thin films. The surface micro-morphology and cross section of our sample could be observed by SEM analysis. Besides, the crystallization of the thin films needed to be investigated directly by XRD analysis. So, SEM analysis is helpful to get enough information to support our illustration. In this study SEM images was performed on a JEOL FESEM JSM6700F instrument

2.5.3 Field Emission Transmission Electron Microscope and Energy Dispersive X-ray Spectrometer

The state-of-the-art JEOL JEM-2100F field emission transmission electron microscope is equipped with an Oxford INCA Energy TEM 200 EDX (energy dispersive X-ray spectrometer) system, a Gatan GIF Tridiem EELS (electron energy loss spectrometer) system and a Fischione high-angle annular dark field detector. Features of the JEM-2100F include a high-brightness Schottky field emission electron gun producing a probe size of less than 0.2 nm. Ultra-high point-to-point TEM resolution is 0.19 nm; atomic scale resolution of 0.136 nm can be achieved using high angle annular dark field (HAADF) scanning transmission electron microscopy (STEM) imaging. The facilities are ideally suited for crystallographic and chemical analyses at a sub-nanometer scale, including high-sensitivity EDX and EELS.

2.5.4 X-ray Photoelectron Spectroscopy (XPS)

XPS is a quantitative spectroscopic technique that measures the elemental composition, empirical formula, chemical state and electronic state of the elements that exist within a material. XPS spectra are obtained by irradiating a material with a beam of X-rays while simultaneously measuring the kinetic energy (KE) and number of electrons that escape from the top 1 to 10 nm of the material being analyzed. XPS requires ultra-high vacuum (UHV) conditions.

XPS is a surface chemical analysis technique that can be used to analyze the surface chemistry of a material in its "as received" state, or after some

treatment such as: fracturing, cutting or scraping in air or UHV to expose the bulk chemistry, ion beam etching to clean off some of the surface contamination, exposure to heat to study the changes due to heating, exposure to reactive gases or solutions, exposure to ion beam implant, exposure to ultraviolet light, for example.

2.5.5 BET analysis

In 1938, Stephen Brunauer, Paul Hugh Emmett, and Edward Teller established the BET theory for the first time, which is a well-known rule for the physical adsorption of gas molecules on a solid or powder surface and serves as the basis for an important analysis technique for the measurement of the specific surface area of a material.

The BET method is widely used in surface science for the calculation of surface areas of solids and powder. A total surface area S_{total} and a specific surface area S are evaluated by the following equations:

$$S_{BET, total} = \frac{v_m N \cdot s}{V} \quad [\text{Eq.2-1}]$$

$$S_{BET} = \frac{S_{BET, total}}{g} \quad [\text{Eq.2-2}]$$

Where N is avoquadro's number, s is adsorption cross section, V is molar volume of adsorbent gas, v_m is the monolayer adsorbed gas quantity, and g is molar weight of adsorbed species.

2.5.6 Thermal Gravimetric Analysis (TGA)

Thermal gravimetric analysis is a type of content testing that is performed on samples to determine changes in weight related to change in temperature. The analyzer usually consists of a high-precision balance with a platinum pan loaded with the sample. The pan is set in a small electrically heated oven with a thermocouple to accurately measure the temperature. In order to protect sample from oxidation or other undesired reactions, the atmosphere purged with an inert gas is required. Due to each substance with its own burning out temperature, analysis is carried out by raising the temperature gradually and record the weight of testing sample against temperature to calculate the weight loss and contents percentage. As many weight loss curves look similar, the weight loss curve may require transformation before results may be interpreted. A derivative weight loss curve can be used to tell the point at which weight loss is most apparent.

2.5.7 Electrochemical Properties Measurement

In this study, we used CH Instrument 618B electrochemical analyzer to measure all electrochemical properties. All the electrochemical testing was carried out in a three electrodes system with a SCE reference electrode, a counter electrode of platinum sheet, and 0.1 M Na₂SO₄ as the electrolyte. This measurement system is illustrated in fig.2-3. There are three measurement tests described as followed from which we can understand the capacitive behaviors of sample.

I . Cyclic Voltammetry Measurement

The most important part of all is cyclic voltammetry measurement. We could understand the electric properties of the device from CV curve. The CV measurement was performed by electrochemical analyzer which applied a DC voltage sweeping between 0 V and 0.8 V at the same scan rate to observe the faradic current of our sample. There were five different scan rates adopted, 5mV/s, 25mV/s, 50mV/s, 75mV/s, and 100mV/s.

II . Stability Test

When sample was tested for several times, the specific capacitance will decrease gradually. How to maintain the specific capacitance is important for supercapacitors. We chose galvanostatic technical mode to measure the stability of sample. The sample was charged and discharged at a constant 1mA current in the voltage window ranging from 0 V to 0.8V for 6000 cycles and each cycle was calculated the degradation and compared with first cycle.

III . Impedance Measurement

Impedance Measurement is a useful method to understand the interface resistances and equivalent circuit for supercapacitors. All the samples in this study were measured at 0.1 V. The amplitude of AC signal was 10 mV and the frequency ranged from 10 mHz to 100 kHz.

	MnO₂/CNTs		MnO₂	
Solution content	Purified CNTs	KMnO₄	Purified CNTs	KMnO₄
		0.4g	0.005M 200ml	/
MnSO₄	0.0016M 90ml drop by drop			
Experiment time	6 hours			
Rotation	300 rpm			
Temperature	Room			

Table 2-1 Synthesis of active material

Chemicals	Manufacturer	Grade
Potassium Permanganate	J.T. Baker	99.0%
Manganese Sulfate Pentahydrate	NACALAI TESQUE, INC.	98.0%
Sodium Sulfate	NACALAI TESQUE, INC.	98.5%
Multi-wall Carbon nanotubes	CNT, CO.	MWCNT
2-Propanol	J.T. Baker	CMOS Electronic 99.5%
Nitride Acid	J.T. Baker	CMOS Electronic 70.0%
Hydrochloric Acid	SIGMA-ALDRICH	37%

Table 2-2 Details of Chemicals used in this experiment

	Sample A	Sample B	Sample C
Current Collector	Ni	CNTs/Ni	Ni
Active Material	MnO _x /CNT	MnO _x	MnO _x
Applied Voltage(V)	30 V 、 40 V	30 V	30 V
Deposition Time(mins)	20 、 40 、 60	20	20
Annealing Temperature(°C)	150 、 200 、 250		

Table 2-3 EPD parameters of all samples in this experiment

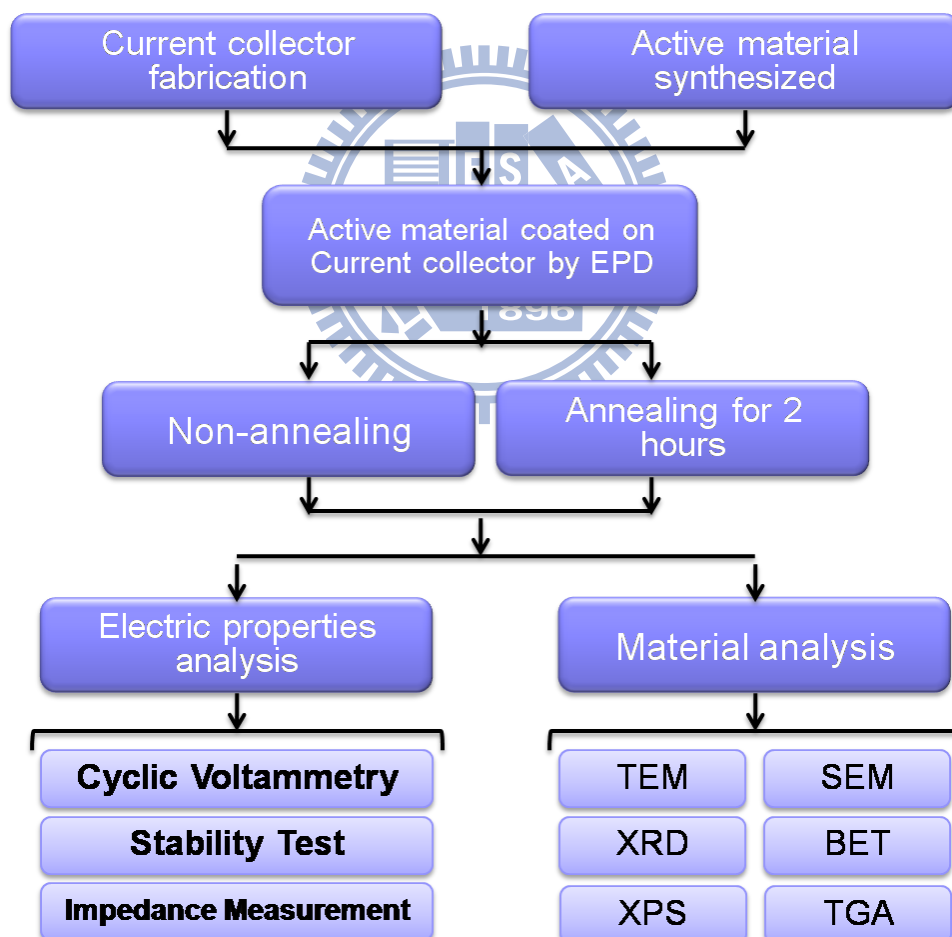


Fig.2-1 Illustration of the experimental flow

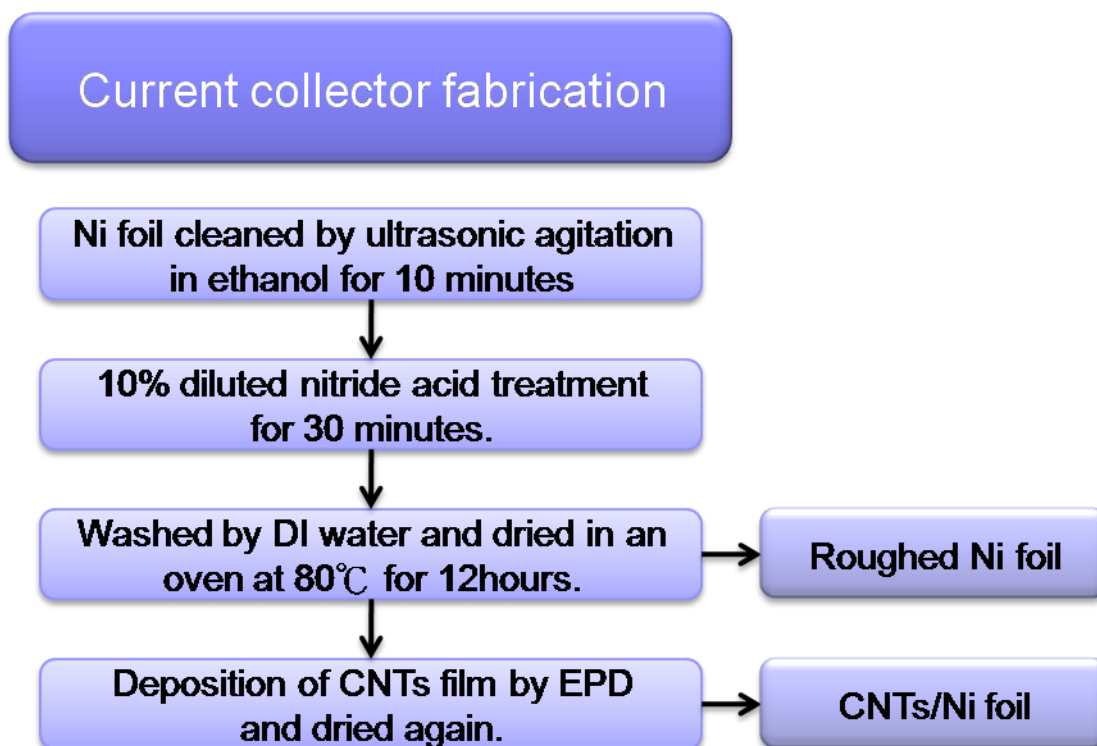


Fig.2-2 Illustration of the current collector fabrication flow

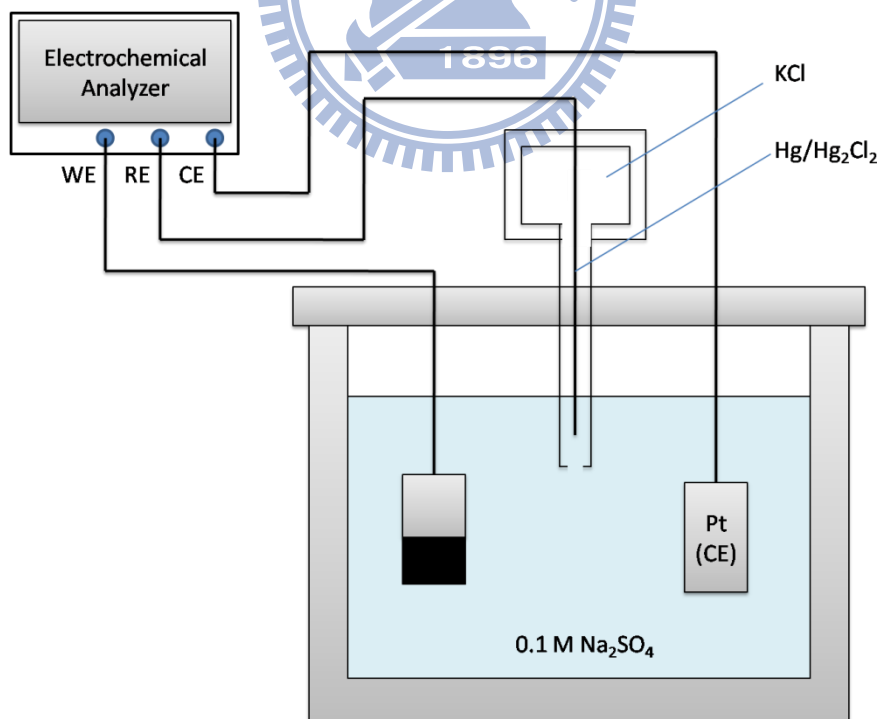


Fig.2-3 Illustration of the electrochemical measurement system

Chapter 3

Results and Discussion

3.1 Supercapacitors Fabrication

Electrophoretic deposition is a potential method to produce supercapacitors with advantages of low cost, safety, and high production rate. According to previous studies, the MnO_x film deposited from Mn^{2+} ions into CNTs/Ni surface had higher capacitance and reversibility than MnO_x/Ni supercapacitors because CNTs increased the surface area and conductivity of electrode³³. Zhitoirsky and his co-worker used adding some polymer as surfactant to electrolyte which ionizes MnO_2 nanowires and CNTs to produce co-deposition MnO_x/CNTs supercapacitors³⁴.

In this study, we substitute H^+ ions for polymer which is considered as a charge transfer resistance for fast redox reaction. Although H^+ ions can ionize the surface group of MnO_x nanoparticles, CNTs can't have charge on their surface for EPD application by absorbing them. Therefore, in order to deposit MnO_x and CNTs simultaneously, a synthesis of coaxial MnO_x/CNTs composite was required in this experiment.

3.1.1 Current Collectors Fabrication

An ideal current collector must have high surface area, good adhesion to deposit film, and inactive to electrolyte during measurement. Nickel is an appropriate candidate for electrode substrate than platinum due to their prices. For supercapacitors, the adhesion between current collector and thin film such as CNTs, MnO_x , and MnO_x/CNT composite will affect their stability of capacitive performance. Nickel foil in this experiment was put in 10% nitride acid to increase surface roughness because the surface nickel was oxidized to green Ni^{2+} ion and dissolved in strong acid. Rough surface provides more contact area for CNTs or active powders so that they can stick on nickel confirmedly³³. Comparing to polish nickel foil, CNTs or active powders can be also coated by EPD method but the thin film will crack or peel off when sample was dried or tested for electrochemical properties.

The purification of CNTs and forming oxygenated group on CNTs surface were achieved by different oxidation rate of impurities and CNTs in 70% boiling nitride acid. Nanotubes treat in this way is well known to have surface negative charges that electrostatically stabilize the aqueous suspensions for long periods. Mg^{2+} absorbed by oxygenated group of CNTs can change the surface charge from negative to positive in IPA. In this study all the applied voltage of electrophoretic deposition were high than 1.23V, water decomposed voltage, which cause a large amount of oxygen and hydrogen bubbles that destroy the deposits qualities and adhesion, so water-free 2-propanol was adopted as EPD solvent.

3.1.2 Electrophoretic Deposition of Active Material

In electrophoretic deposition process hydrogen ions when the pH value of electrolyte below 7 served as surface charge additive that ionizes the nanostructure of manganese oxide to stabilize the suspension. The ratio of 37% hydrochloric acid containing water to 2-propanol was limited due to the voltage of hydrolysis. We found that when the volume ratio above 1/5000 the qualities of deposit were destructed by hydrogen bubbles. It is also very important for active material deposition to choose a suitable applied voltage because the electric field between two electrodes during EPD forces active material with positive charge to move to cathode. When electric field was below 20V/cm, we can't attach the deposits to current collector firmly. The deposited film will be stripped by sprinkling DI water on its surface.

3.2 Material Analyses of MnO_x Nanopowder and MnO_x/CNTs Composite

Two kinds of nanopowder, MnO_x and MnO_x/CNTs composite, as active materials were produced in this experiment. Both manganese oxides were formed from potassium permanganate and manganese sulfate. When manganese sulfate solution added into a violet aqueous liquid containing potassium permanganate that is well known as a strong oxidant, Mn²⁺ from manganese sulfate was oxide into MnO_x and potassium permanganate also transferred into MnO_x due to reduction.

The figure 3-1 and 3-2 are TEM image of MnO_x and MnO_x/CNTs composite, respectively. For MnO_x nanopowder, the diffraction pattern indicates that the structure is amorphous. Figure 3-2 tell us that MnO_x/CNTs composite has coaxial structure with 3~4nm manganese oxide on CNTs. The atoms of manganese oxide in this TEM image are not in an ordered arrangement which means that manganese oxide on the CNTs is amorphous structure.

The specific area considered as the effective place of fast redox reaction was also measured by BET method in this study. Table 3-1 are the measurement result described as following: CNTs with $40\sim 300\text{m}^2/\text{g}$, purchased from CNT, CO., was calculated as $131.3\text{ m}^2/\text{g}$ and MnO_x nanopowder and MnO_x/CNTs composite were 59.5 and $170.9\text{ m}^2/\text{g}$, respectively. The result from BET measurement showed the evidence that conformal MnO_x film precipitating on CNTs surface will enhance the specific area nearly 3 times than it of MnO_x nanopowder due to CNTs extending the deposit area per weight of manganese oxide. High specific area allows more available manganese oxide to exchange ions from electrolyte leading to a high specific capacitance. The electrochemical performances of these powders are carried out in the next section.

Figure 3-3 is thermal gravimetric analysis for MnO_x/CNTs composite according to the DSC curve of fig. 3-3, the exothermal peak around 380°C can be assigned to the ignition of carbon naotubes resulting in 68% weight loss of the composite. Some weight loss below 250°C in the curve can be attributed to the evaporation of physically adsorbed water.

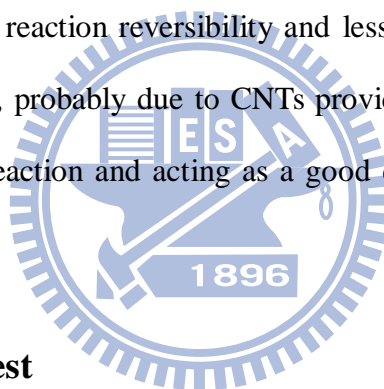
3.3 Electrochemical properties of MnO_x nanopowder and MnO_x/CNT composite

3.3.1 Cyclic Voltammerty Measurement

We used cyclic voltammerty method to measure the electrochemical performances of supercapacitor at five different scanning rates, 5mV/s, 25mV/s, 50mV/s, 75mV/s, and 100mV/s. Three different structures of supercapacitors mentioned in chapter 2, MnO_x/CNTs on nickel, and MnO_x on nickel or CNTs/nickel substrate, will be discussed in this section. All the weight of samples were controlled within $45 \pm 5 \mu\text{g}$ by adjusting the deposition time at 30V. At first, observing from SEM images shown in fig.3-4 to fig.3-6, we can find out that the precipitation of sample C became a dense layer due to the low specific area of MnO_x nanopowder and nickel substrate. The substrate of sample B had a CNTs layer to extend surface area which permitted MnO_x nanopowder to deposit dispersedly so that sample B had much available contact surface with electrolyte to charge and discharge. Besides CNTs could enhance the conductivity of supercapacitors because it spread MnO_x nanopowder thought of as high resistance to decrease the thickness of manganese oxide which was between current collector and electrolyte. The SEM of sample A shows a large amount of composite material tangled to form a porosity layer. Since MnO_x/CNTs composite had larger specific area, we assumed that it also had better electrochemical performances.

Figure 3-7 to 3-9 shows the CV curves of these three samples in 0.1 M Na₂SO₄ solution cycled under a potential in the range from 0 to 0.8 V and

figure 3-10 overlaps these CV curves with a scan rate of 100mV/s. The CV curves of sample A and B with CNTs are almost rectangular in shape, which implies that both of them exhibit capacitive behavior. All the measured specific capacitances are shown in the fig.3-11 and listed in detail in table 3-2. From them we can find that the specific capacitances of these samples decrease as the potential scan rate increases. As the potential scan rate is raised to 100 mV/s, the specific capacitance of the sample C decreases to 166 F/g, which is 69.7% of that measured with a scan rate of 5 mV/s, whereas the specific capacitance of sample A and B is 378 F/g and 306 F/g, which are 78.8% and 81.2%, respectively, of that measured with a scan rate of 5 mV/s. Sample A and B with CNTs exhibit good reaction reversibility and less capacitance decay for faster potential scan rates, probably due to CNTs providing a large activated surface area to the redox reaction and acting as a good conductor with a low contact resistance.



3.3.2 Stability Test

The electrochemical stability of the electrode was investigated by applying 1mA constant current measurements. Figure 3-12 shows the plots of the maintenance of specific capacitance of these three samples vs. the cycle of the constant current test. The specific capacitances of sample B and C fall to 83.9% and 83.7% of the original value after 1000 cycles of CC test, respectively. However after 3000 cycle tests, the specific capacitance of sample B drops quickly to 37.6% of the original value, which is lower than it of sample C which maintains 71% of the original value. But those of the sample A, MnO_x/CNTs composite on nickel, have less reduction; the capacitances are

93.3% and 84.9% after 1000 and 3000 cycles of tests, respectively. The capacitance of MnO_x/CNTs composite on nickel remains at 79% of the original value until 6000 cycles of CC test. The CC tests indicate that the MnO_x/CNTs composite electrode shows good electrochemical characteristic and stability.

Figure 3-13 is the SEM image of MnO_x/CNTs composite electrode after 6000 cycles which can remain the surface morphology and has low degradation of specific capacitance, probably due to better adhesion between manganese oxide and CNTs that reduce the dissolution of MnO_x film. However, as shown in figure 3-14 and 3-15, the SEM planar view images of sample B and C after 3000 cycles pointing that the MnO_x nanopowder layer after a long constant current cycling will peel out because it follows a dissolution-redeposition mechanism^{56,57}. When measuring from 0.8V to 0V, the MnO₂ nanopowder will be reduced and some will be dissolved into the electrolyte as Mn²⁺ cations⁵⁸. And scanning from 0V to 0.8V, some of the dissolved Mn²⁺ cations will transform into MnO₂ and deposit on the electrode surface again. Increasing the cycle number, a sequential dissolution-redeposition reaction for manganese oxide makes the morphology and become totally different than its original. We believed that the structure with lower specific area and lost some dissolved manganese oxide cause specific capacitance of sample B and C to decay quickly when sample measured for a long cycle number.

3.4 Different Deposition Time and Voltage of MnO_x/CNT composite

Since MnO_x/CNTs composite electrode has excellent electrochemical properties, we concern about that how does the electrochemical characterization change when the applied different deposition time and voltage. Figure 3-16 is the cross section images of composite electrode fabricated at 30V for 20, 40, 60 minutes whose weigh are 27.2, 47.5, 75.7 μ g and thickness are 0.817, 1.167, 1.370 μ m and at 40V for 20, 40, 60 minutes whose weigh are 31.5, 74.1, 131.3 μ g and thickness are 1.235, 1.53, 1.757 μ m, respectively, as listed in table 3-3. It is obvious to distinguish that the thickness become thicker when increasing the deposition time

The cyclic voltammometry test for composite electrode applied 30V and 40V for 20, 40, and 60 minutes are shown in fig.3-17 to 3-18 and table 3-4. From figure 3-19 the capacitances of all samples at 100mV/s can maintain above 75% of that they were tested at 5mV/s and we can find that the specific capacitances in the same EPD voltage decay when deposition time increased because the Na⁺ ion can't penetrate into the inner layer of thicker deposit film to be stored in a short reaction time. Therefore deposited for 20mins sample has highest specific capacitance, 417/g for 30V-20mins and 621F/g for 40V-20mins at 100mV/s. While comparing with different EPD voltage, the specific capacitance of 40V-20mins is higher than it of 30V-20mins although the weights of both are closed. It is the same case for 40V-40mins and 30V-60mins, because samples at 40V have thicker layer so that they have much lower density of deposit. In other words, they are more porous allowing Na⁺ to

insert and deinsert into MnO_x in deep layer. Table 3-3 and figure 3-20 show that the specific capacitance is decayed when the density of deposited film increased.

3.5 Thermal annealing of MnO_x/CNT composite

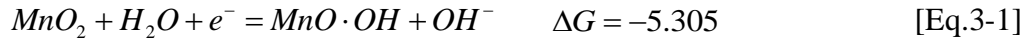
We assumed that the stability of composite supercapacitors is based on the adhesion between manganese oxide and carbon nanotubes. In order to know how thermal treatment to affect their stability and specific capacitance, we annealed MnO_x/CNTs composite supercapacitors at 150°C , 200°C , and 250°C for 2 hours.

3.5.1 Cyclic Voltammerty Measurement

The specific capacitances were also measured at five different scanning rates by CV method and their specific capacitances at 100mV/s are shown in fig.3-21 to 3-22. From table 3-5, as the temperature raises, the value of specific capacitance has a significant upgrade. For $40\text{V}-20\text{mins}$, its specific capacitance is 699F/g without annealed and 771F/g , 846F/g and 840F/g a scanned at 5mV/s when annealed at 150°C , 200°C , and 250°C respectively. Moreover, the specific capacitance at high scanning rate still keeping nearly 80% of that measured at 5mV/s shows that MnO_x/CNTs composite supercapacitors, whether they are annealed or not, have excellent property of fast electrochemical reaction.

3.5.2 Material Analyses

Figure 3-23 is the XRD analysis of MnO_x/CNTs composite in different temperature. The three peaks, 44.5, 51.9, and 76.5, are nickel substrate signals. No noticeable peaks of manganese oxide indicate it still remains amorphous which is an appropriate structure for the rapid oxidation-reduction reaction. From Mn_{3/2P} XPS analysis as shown in fig.3-24 and table 3-6, we can find that the manganese oxide is composed of Mn₃O₄ and MnO₂. From the following chemical reactions at 25°C:



While hydrated manganese oxide, MnOOH, is an adequate material to charge and discharge for supercapacitor storage mechanism from Eq.1-3. Therefore With increasing annealing temperature, the content of MnO₂ is also increased from 65.3% without thermal annealing to 80.1% after annealed at 250°C for 2 hours that prefers transforming into MnOOH by which the specific capacitance of composite is enhanced.

3.5.3 Impedance Analysis

The impedance results in different annealing temperatures, as shown in fig.3-25, containing a semicircle and a nearly 45° straight line at low frequency which is similar to ideal supercapacitors have an evidence that the radius of semicircle is declined when temperature increased. It means that the reduction of charge transfer resistance R_{ct} that is considered as a barrier of Na⁺ insertion/deinsertion lead to more manganese oxide available to charge and

discharge during cycling. From impedance analysis the increase in specific capacitance after thermal treatment can be referred to enlargement of suitable redox sites for Na^+ ions.

3.5.4 Stability Test

In section 3.3.2 we mentioned that MnO_x/CNTs composite supercapacitor is more stable than MnO_x supercapacitors when cycling. Figure 3-27 show that all the specific capacitance produced at 30V and 40V can maintain above 70% of its original after 6000 cycles which indicates that ionizing manganese oxide by H^+ is a useful method to fabricate supercapacitors with high stability without annealed. The mechanism of degradation of capacitance is dissolution of manganese oxide on the carbon nanotube. 30V-20mins without annealed after tested for 6000 cycles, the thickness of manganese oxide decreased to about 2 nm, as shown in fig.3-26 by TEM.

The stabilities of composite electrodes after thermal treatment, as illustrated in fig. 3-28 to 3-30, are promoted when increasing annealing temperature probably due to better adhesion of the structure of MnO_x and CNT. In table 3-7 we can find that all sample with 150°C and 200°C thermal treatment after 6000 tests has more than 80% of its original capacitance in the first cycle except 30V-20mins. All of them can maintain above 80% after annealing at 250°C and the highest can reach 89.1% after 6000 cycles.

Powder	Specific surface area (m²/g)
CNTs	131.33
MnO_x	59.46
MnO_x/CNTs	170.88

Table 3-1 BET specific surface area analysis



scan rate (mV/s)	(A)MnO _x /CNTs on Ni		(B)MnO _x on CNTs/Ni		(C)MnO _x on Ni	
	Capacitance (F/g)	%	Capacitance (F/g)	%	Capacitance (F/g)	%
5	480	100	377	100	238	100
25	432	90.0	330	87.5	187	78.6
50	411	85.6	318	84.3	177	74.3
75	393	81.8	315	83.5	169	71.0
100	378	78.8	306	81.2	166	69.7

Table 3-2 The specific capacitances of three different structures

Voltage	Time(min)	Thickness (nm)	Weight(μg)	Density(g/cm^3)	Specific capacitor(F/g) @ 100mV/sec
30V	20	817	27.2 \pm 2.0	0.33	417
	40	1167	47.5 \pm 5.7	0.41	378
	60	1370	75.7 \pm 7.6	0.55	291
40V	20	1235	31.5 \pm 6.0	0.26	621
	40	1530	74.1 \pm 10.6	0.48	324
	60	1757	131.3 \pm 21.7	0.75	258

Table 3-3 Specific capacitance verses density of deposit by adjusting EPD time and voltage



Voltage	Time(min)	5mV/s	25mV/s	50mV/s	75mV/s	100mV/s
30V	20	486	441	429	423	417
	40	480	432	411	393	378
	60	342	315	303	294	291
40V	20	699	666	645	633	621
	40	393	351	339	330	324
	60	315	276	267	261	258

Table 3-4 Specific capacitances of MnO_x/CNT composite in various EPD parameters

Sample	Temp.	5mV/s	25mV/s	50mV/s	75mV/s	100mV/s
30V-20m	25°C	486	441	429	423	417
	150°C	561	516	492	477	465
	200°C	613	574	564	559	554
	250°C	620	513	499	496	493
30V-40m	25°C	480	432	411	393	378
	150°C	504	450	429	414	402
	200°C	542	471	461	450	445
	250°C	550	483	477	472	469
30V-60m	25°C	342	315	303	294	291
	150°C	363	330	318	309	306
	200°C	408	360	354	348	336
	250°C	412	358	353	350	347
40V-20m	25°C	699	666	645	633	621
	150°C	771	702	681	663	648
	200°C	846	762	744	732	723
	250°C	840	742	723	716	706
40V-40m	25°C	393	351	339	330	324
	150°C	405	369	357	345	339
	200°C	435	409	387	381	372
	250°C	435	381	372	351	348
40V-60m	25°C	315	276	267	261	258
	150°C	315	285	276	267	261
	200°C	333	306	297	291	285
	250°C	342	303	291	282	273

Table 3-5 Specific capacitances of MnO_x/CNT composite after annealed for 2 hours

Temperature	Species	Area%
25°C	MnO ₂	65.3%
	Mn ₃ O ₄	34.7%
150°C	MnO ₂	70.8%
	Mn ₃ O ₄	29.2%
200°C	MnO ₂	81.1%
	Mn ₃ O ₄	18.9%
250°C	MnO ₂	80.1%
	Mn ₃ O ₄	19.9%

Table 3-6 XPS analysis of Mn₂P_{3/2}

Voltage	Time (min)	Room	150°C 2Hr	200°C 2hr	250°C 2hr
30V	20	73.0%	74.7%	79.5%	83.9%
	40	79.0%	81.8%	85.5%	84.7%
	60	78.5%	84.4%	86.9%	89.1%
40V	20	82.8%	81.8%	86.6%	88.4%
	40	74.6%	81.7%	88.5%	84.9%
	60	78.0%	81.2%	86.3%	83.8%

Table 3-7 1mA constant current stability test of MnO_x/CNT composite electrodes after annealed for 2 hours

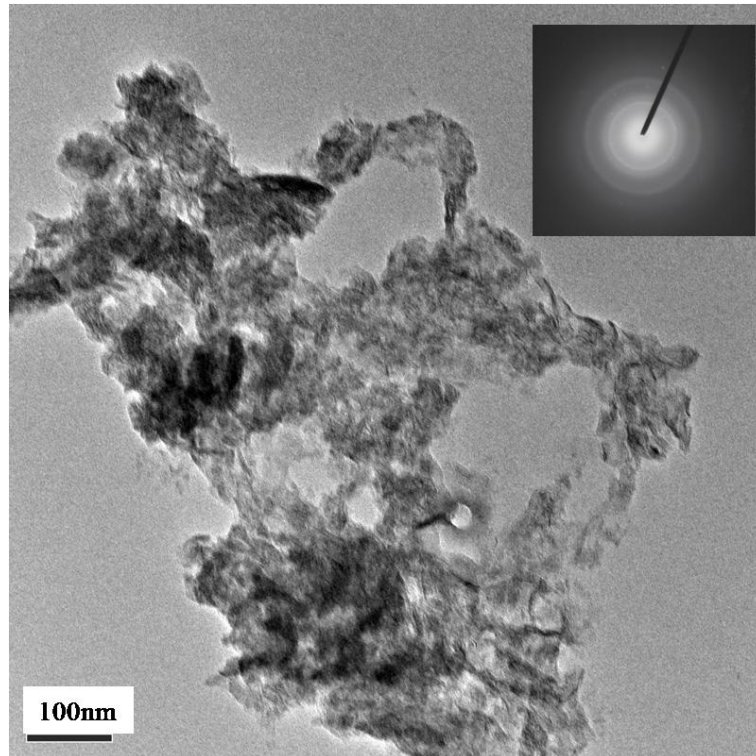


Fig.3-1 TEM image of MnO_x nanoparticle

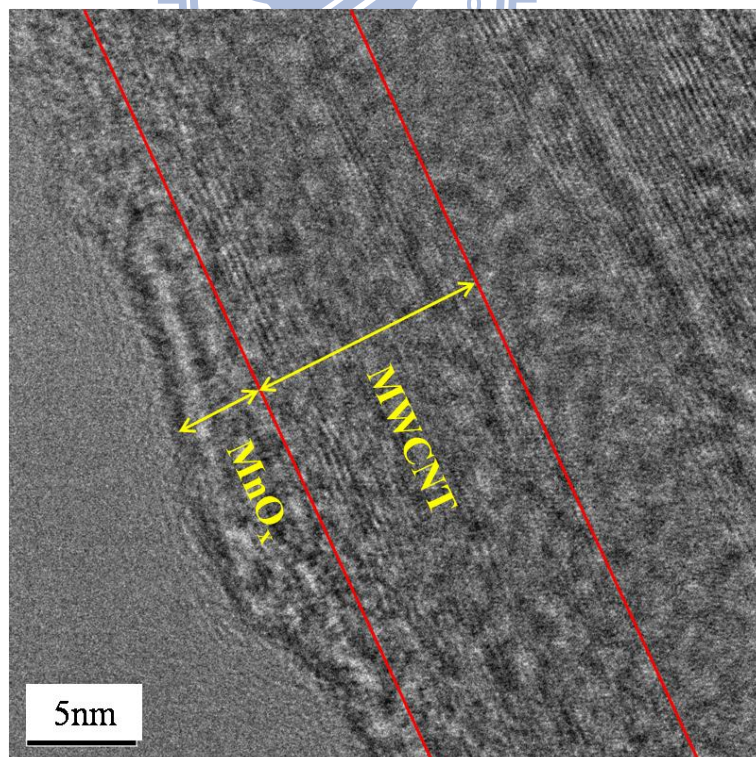


Fig.3-2 TEM image of MnO_x/CNT coaxial composite

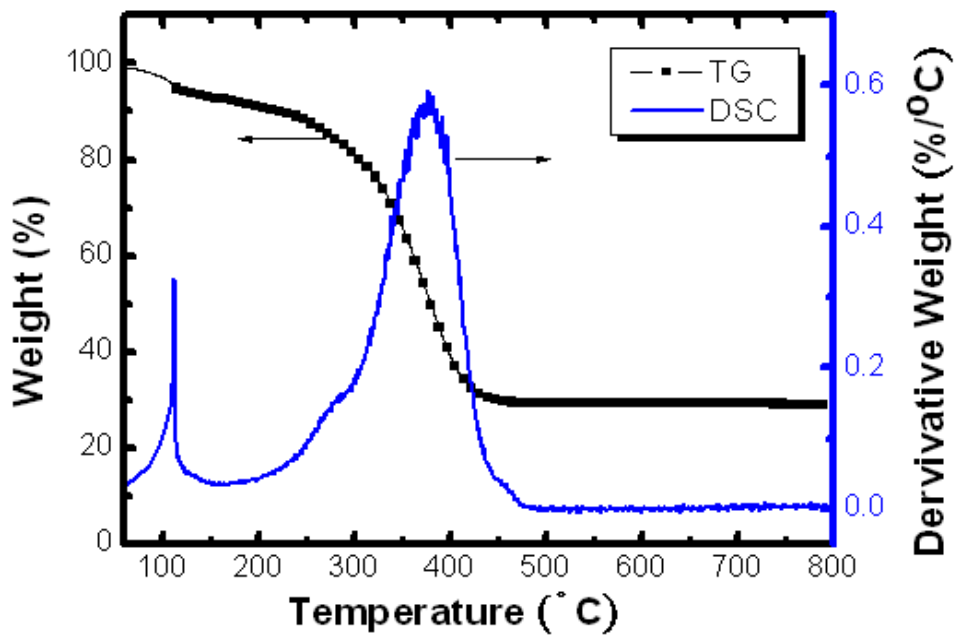


Fig.3-3 Thermal gravimetric analysis for MnO_x/CNT composite

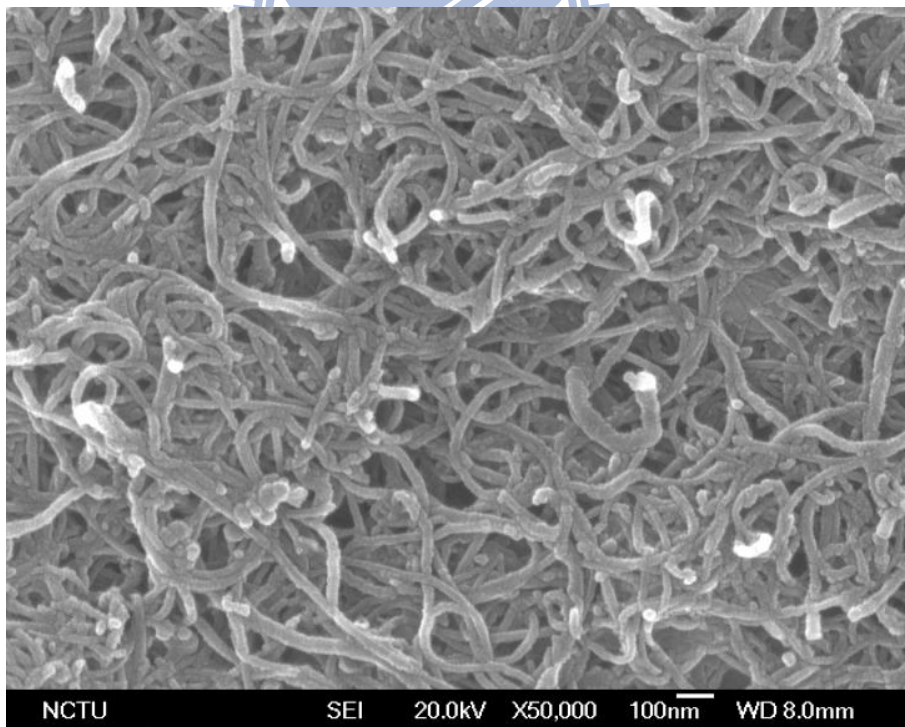


Fig.3-4 SEM image of MnO_x/CNT composite on Ni foil

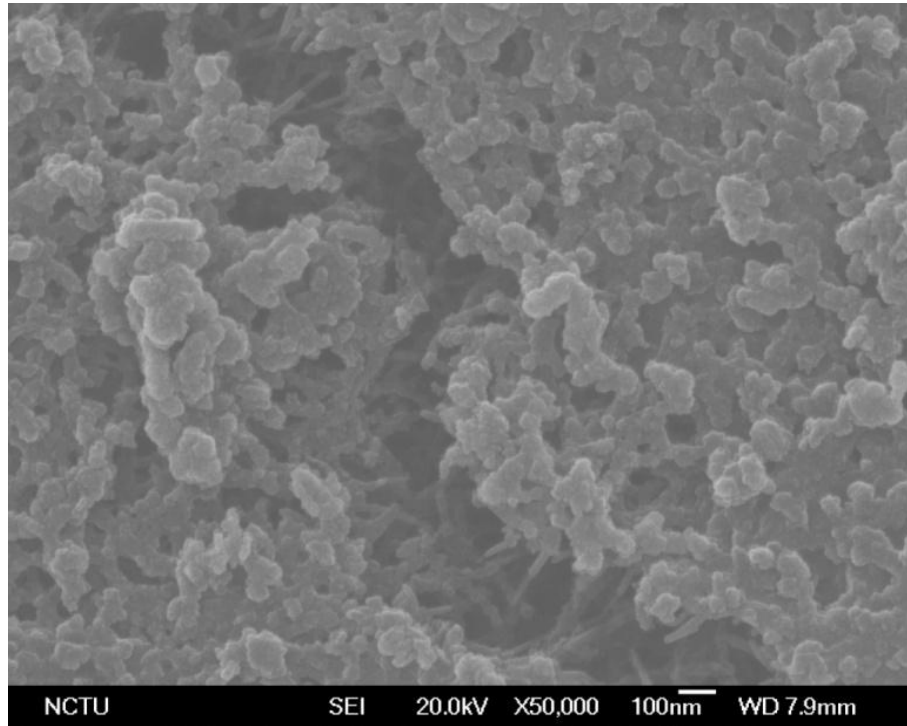


Fig.3-5 SEM image of MnO_x on CNTs/Ni foil

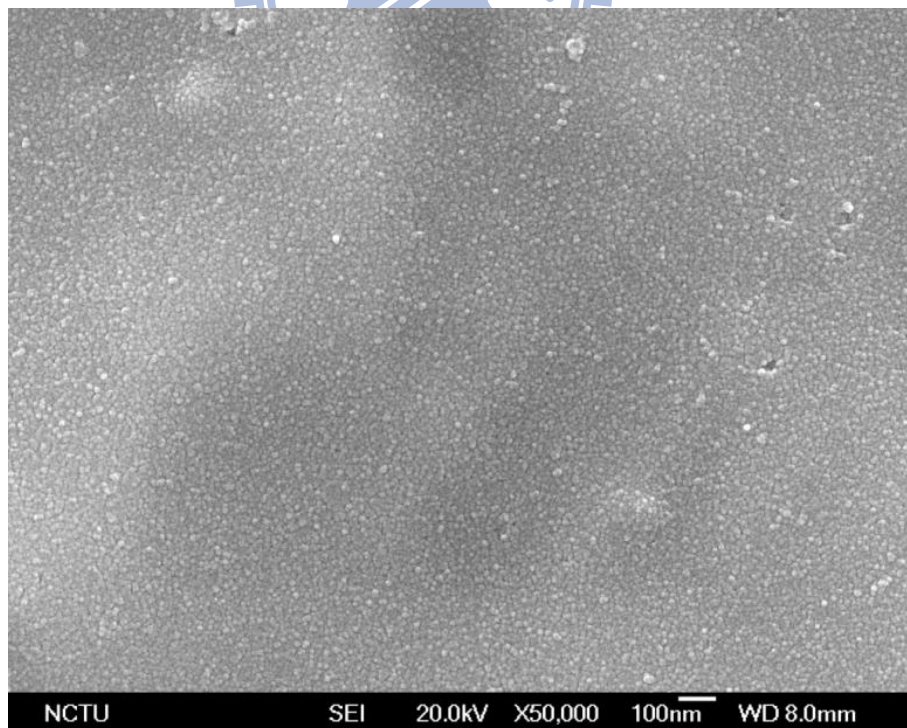


Fig.3-6 SEM image of MnO_x on Ni foil

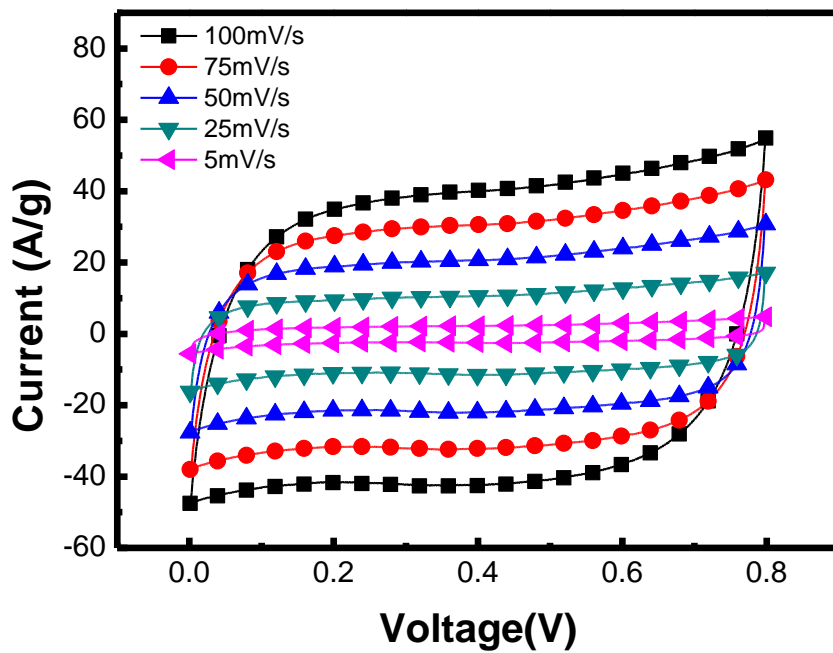


Fig. 3-7 The CV curves of MnO_x/CNTs composite on Ni foil

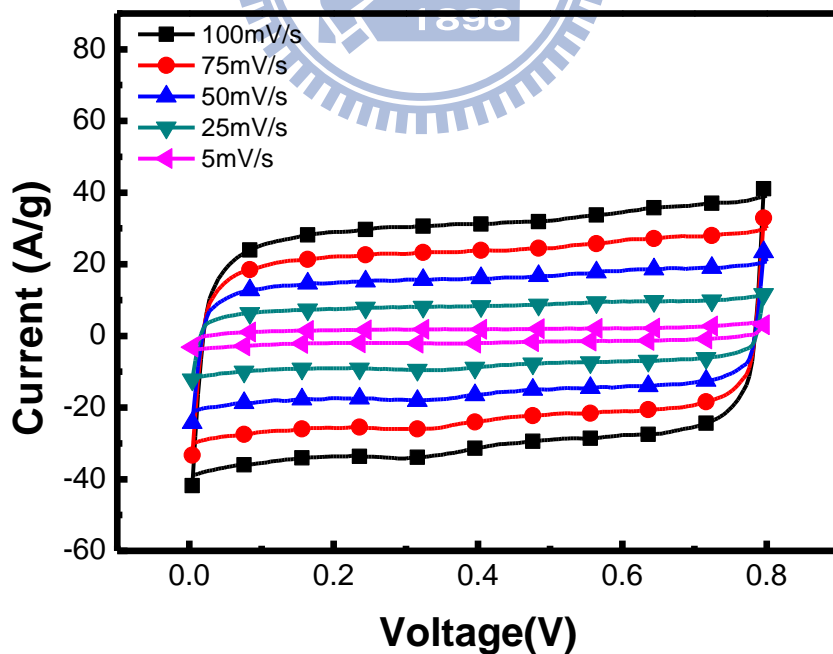


Fig. 3-8 The CV curves of MnO_x on CNTs/Ni foil

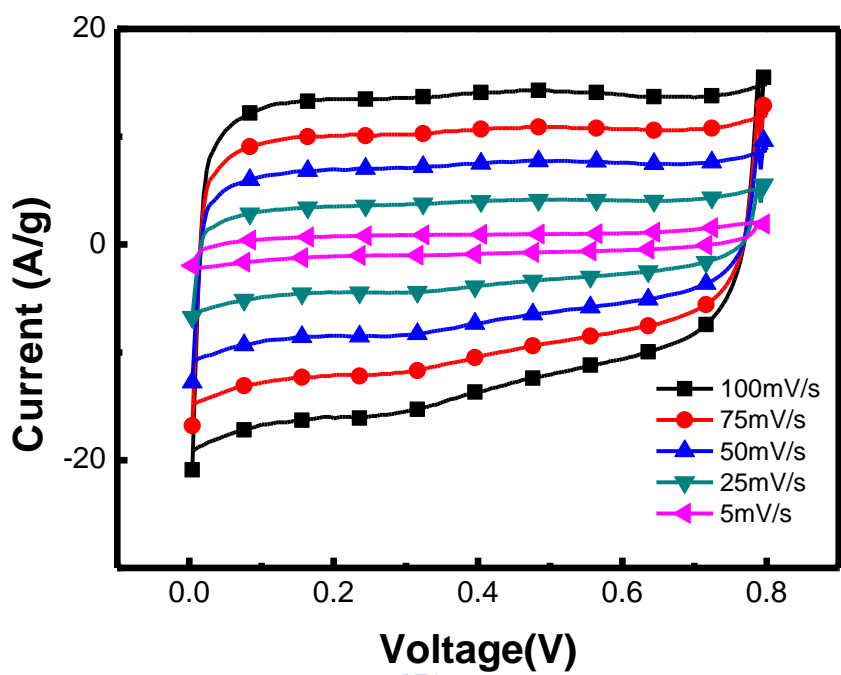


Fig. 3-9 The CV curves of MnO_x on Ni foil

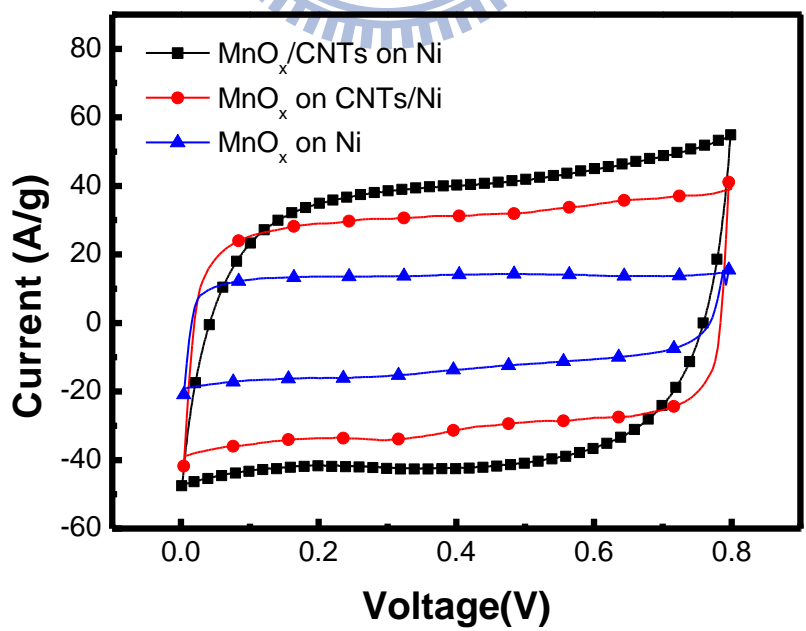


Fig. 3-10 The CV curves of three different structures scanned at 100mV/s

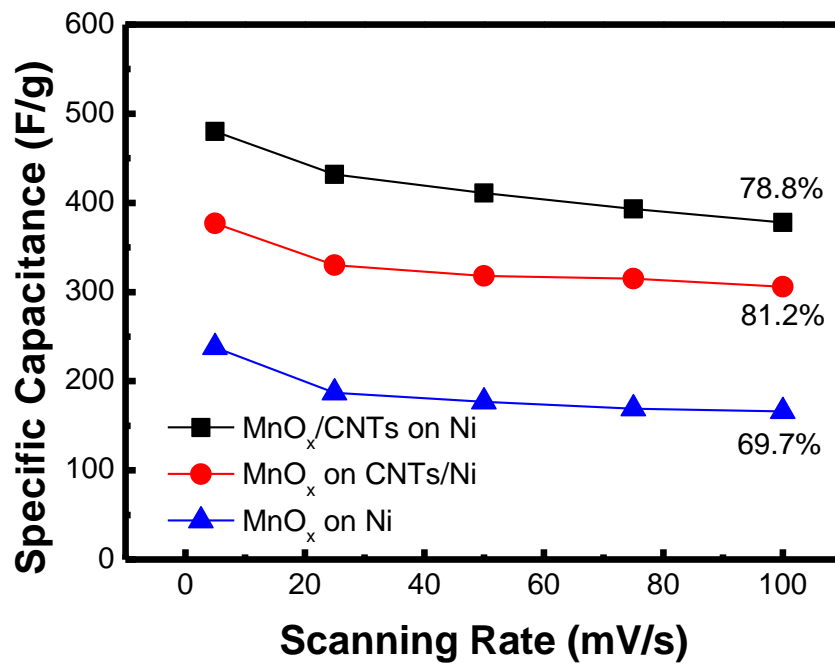


Fig. 3-11 The specific capacitance of three different structures versus scanning rates

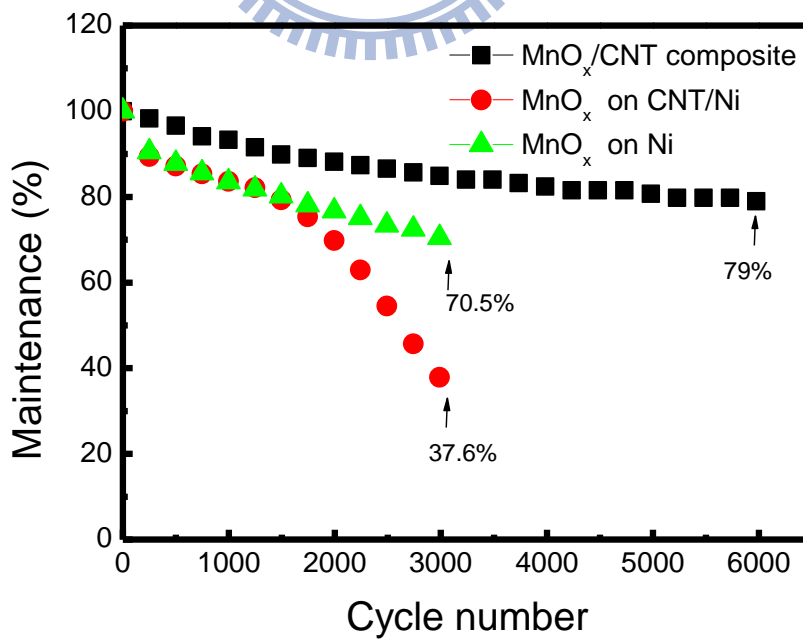


Fig.3-12 Stability test of three different structures

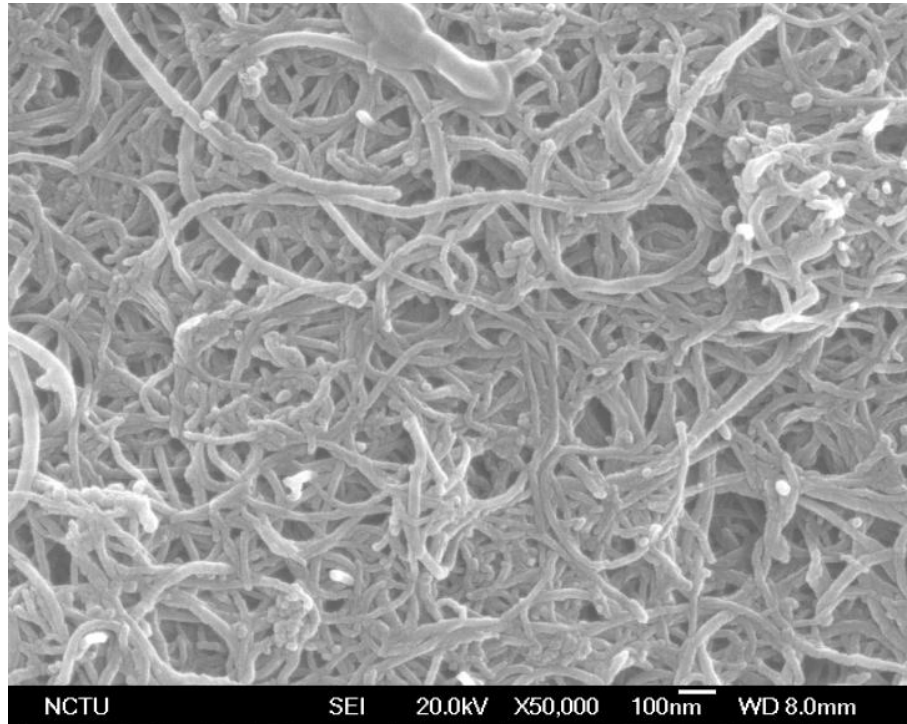


Fig.3-13 SEM image of MnO_x/CNTs composite on Ni foil after 6000 cycles

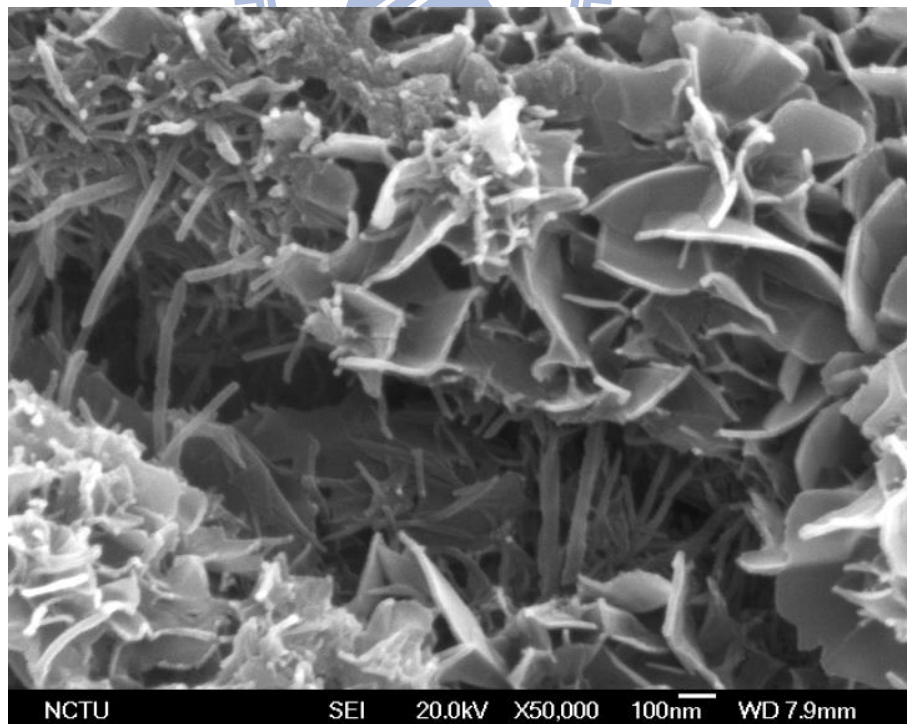


Fig.3-14 SEM image of MnO_x on CNTs/Ni foil after 3000 cycles

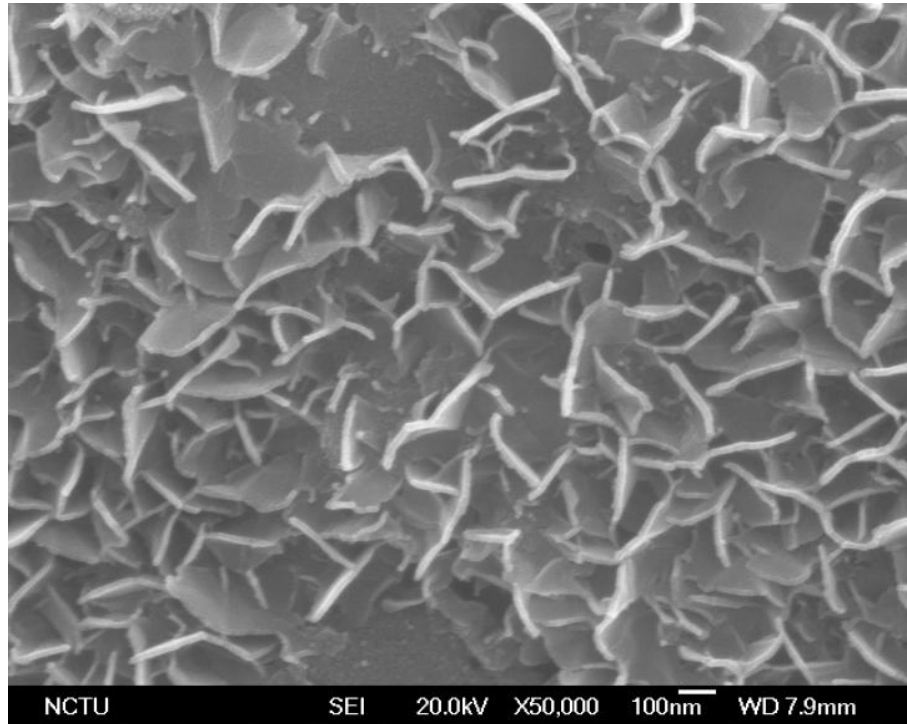


Fig.3-15 SEM image of MnO_x on Ni foil after 3000 cycles



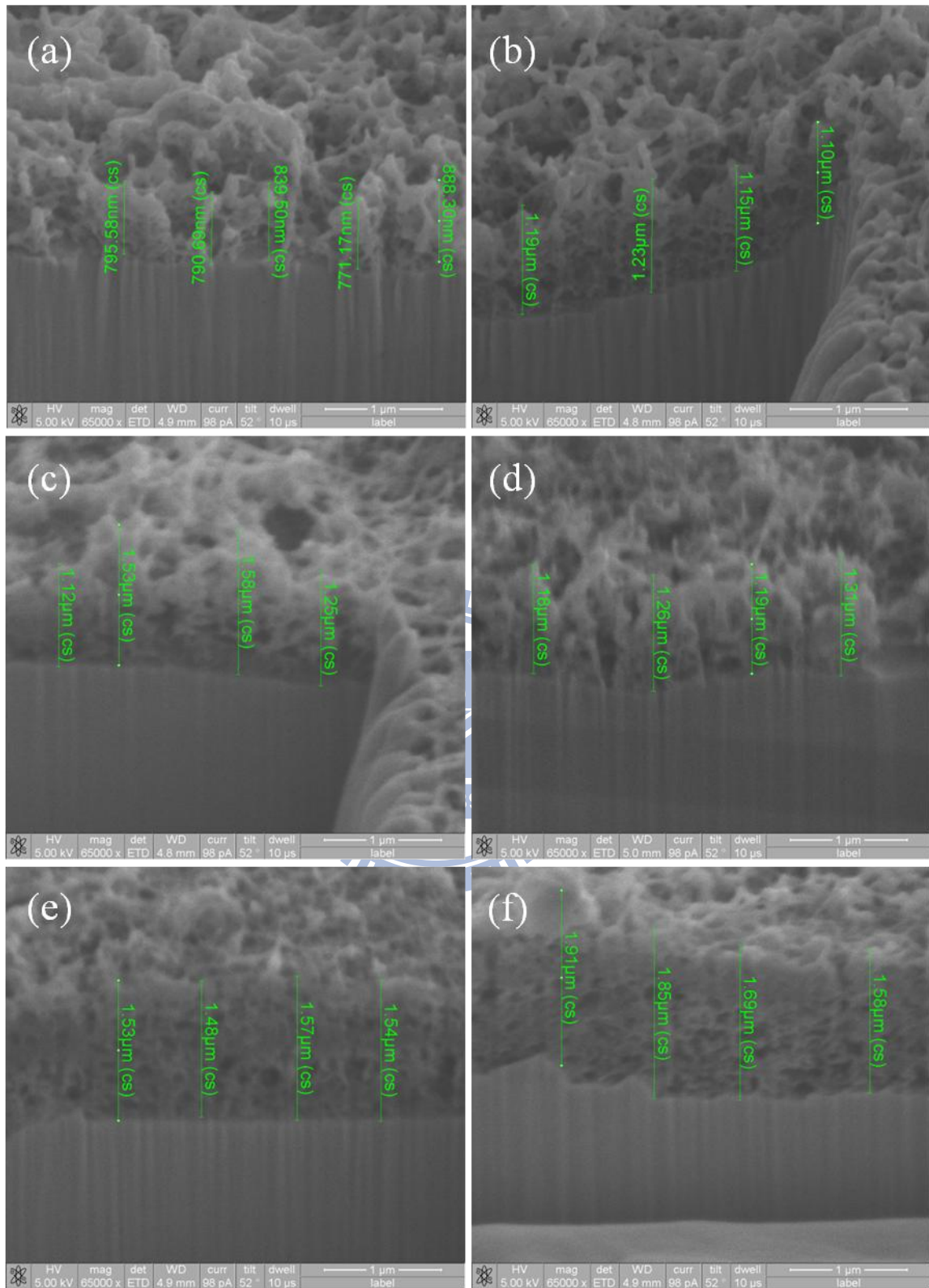


Fig.3-16 Cross section image of (a)30V-20mins (b)30V-40mins (c)30V-60mins (d)40V-20mins (e)40V-40mins (f)40V-60mins by FIB

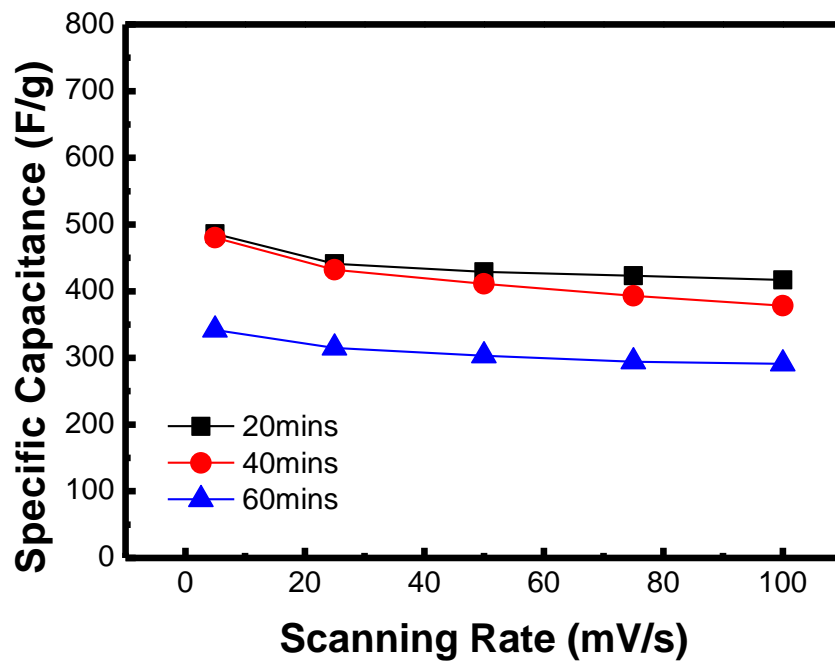


Fig.3-17 Specific capacitance of MnO_x/CNTs composite deposited at 30V

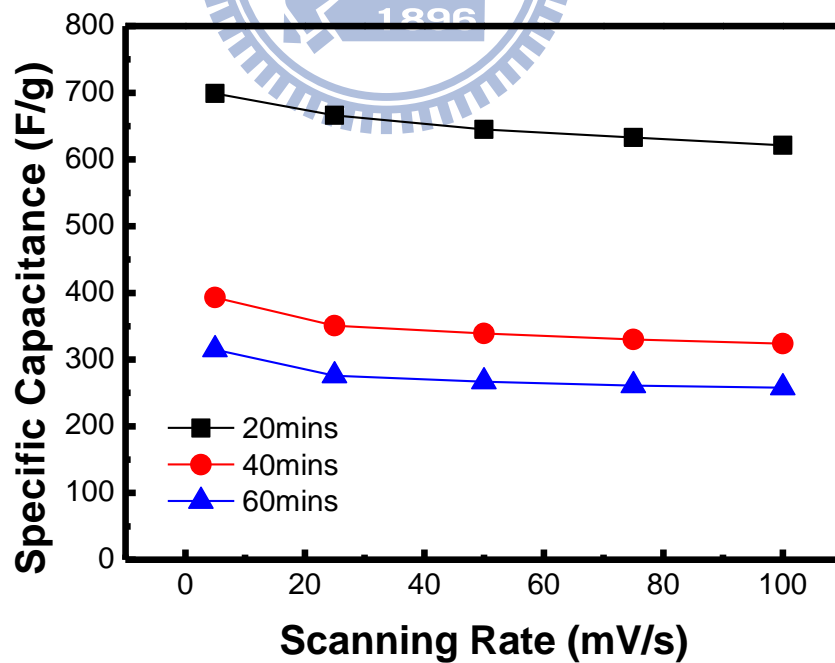


Fig.3-18 Specific capacitance of MnO_x/CNTs composite deposited at 40V

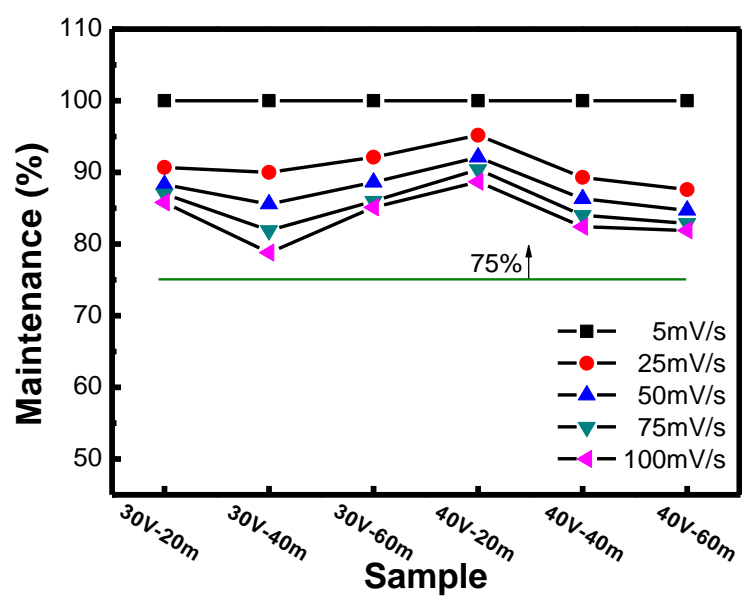


Fig.3-19 The maintenances of specific capacitance of MnO_x/CNTs composite electrodes at different scanning rates

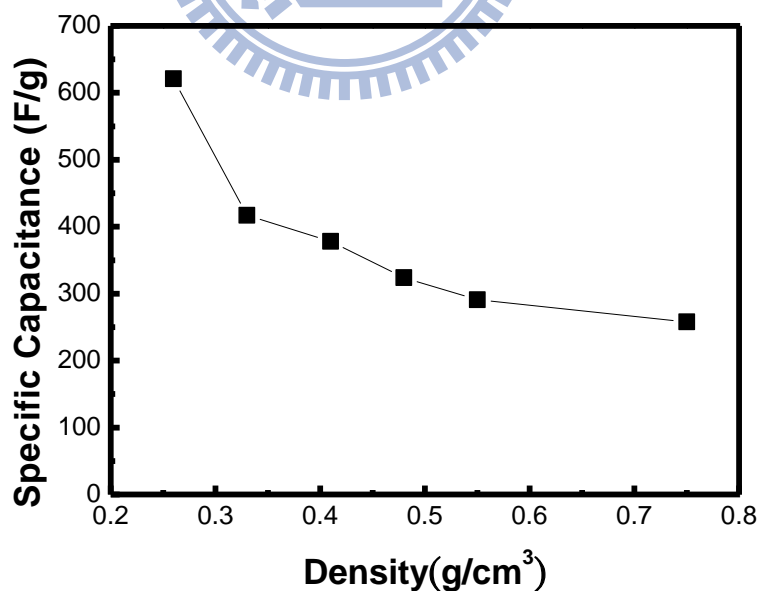


Fig.3-20 The diagram of specific capacitance at 100mV/s verse the density of deposits

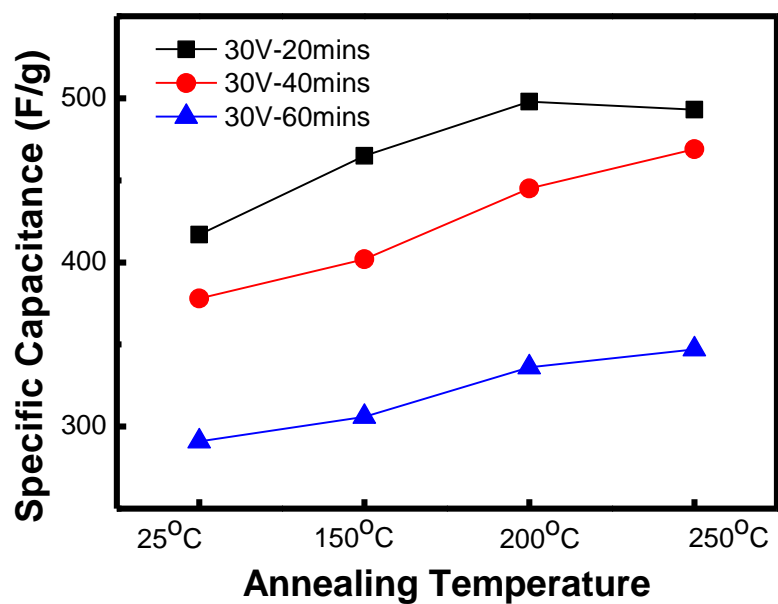


Fig.3-21 Specific capacitance at 100mV/s of MnO_x/CNTs composite deposited at 30V after thermal annealing for 2 hours

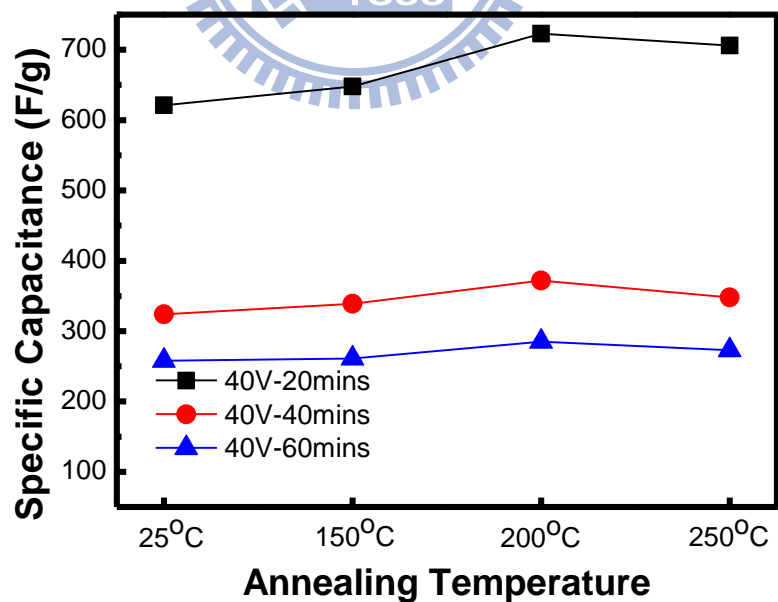


Fig.3-22 Specific capacitance at 100mV/s of MnO_x/CNTs composite deposited at 40V after thermal annealing for 2 hours

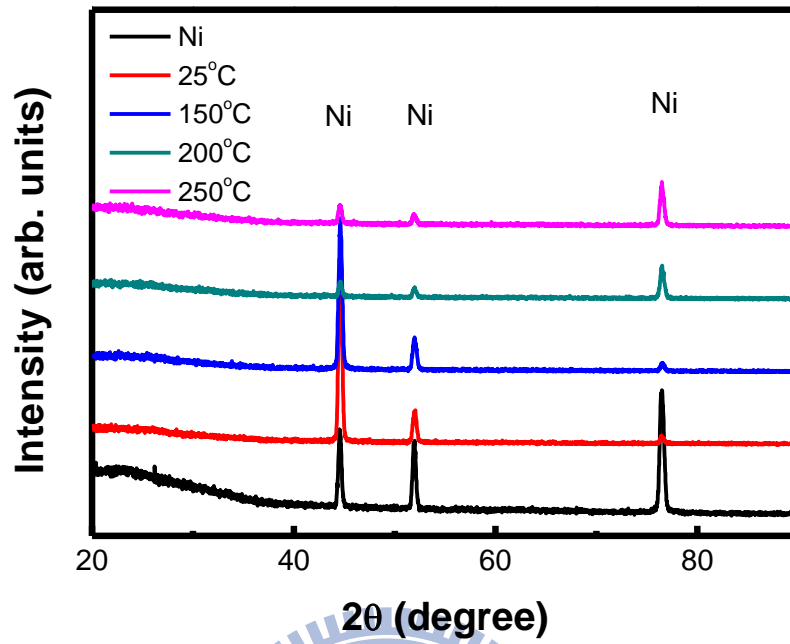


Fig.3-23 XRD of MnO_x/CNTs composite electrodes after thermal annealing

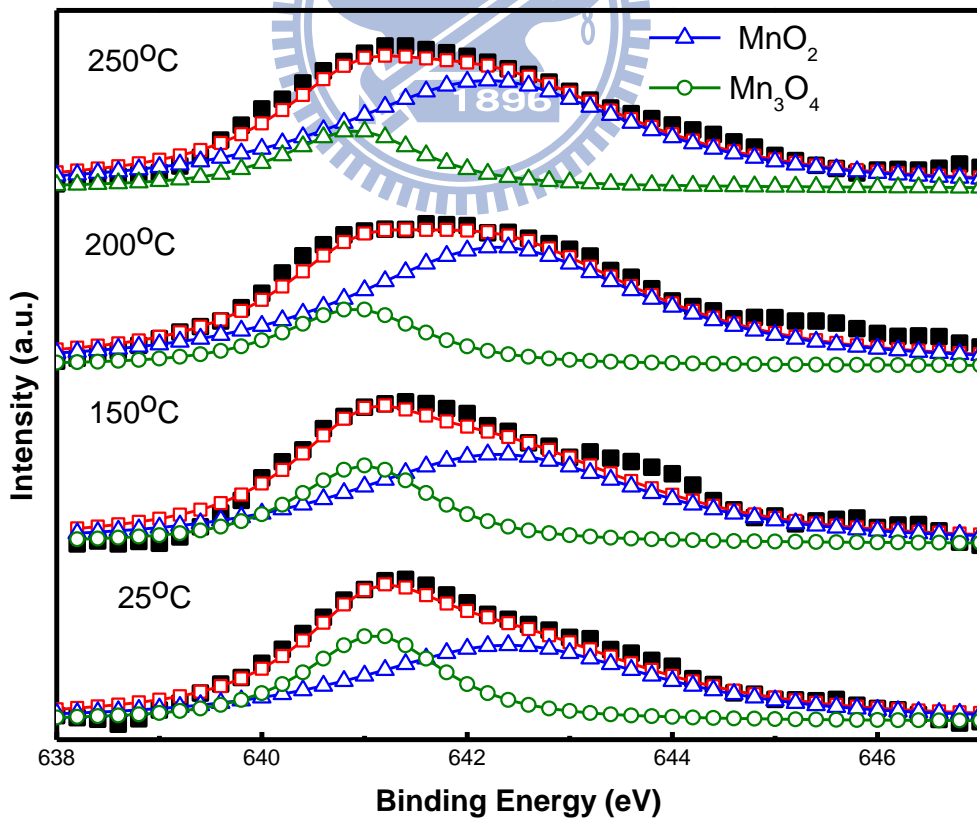


Fig.3-24 XPS of MnO_x/CNTs composite electrodes after thermal annealing

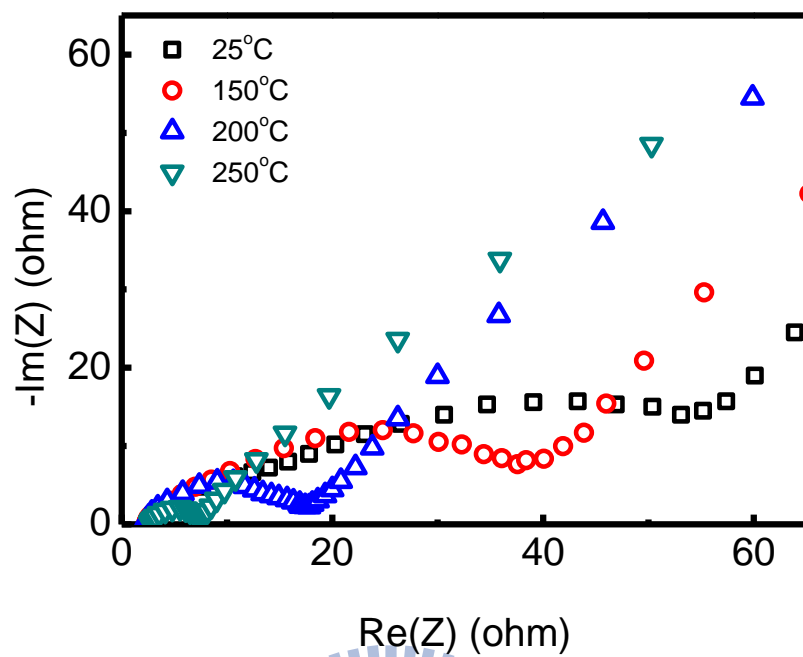


Fig.3-25 Impedance analysis of $MnO_x/CNTs$ composite electrodes after thermal annealing

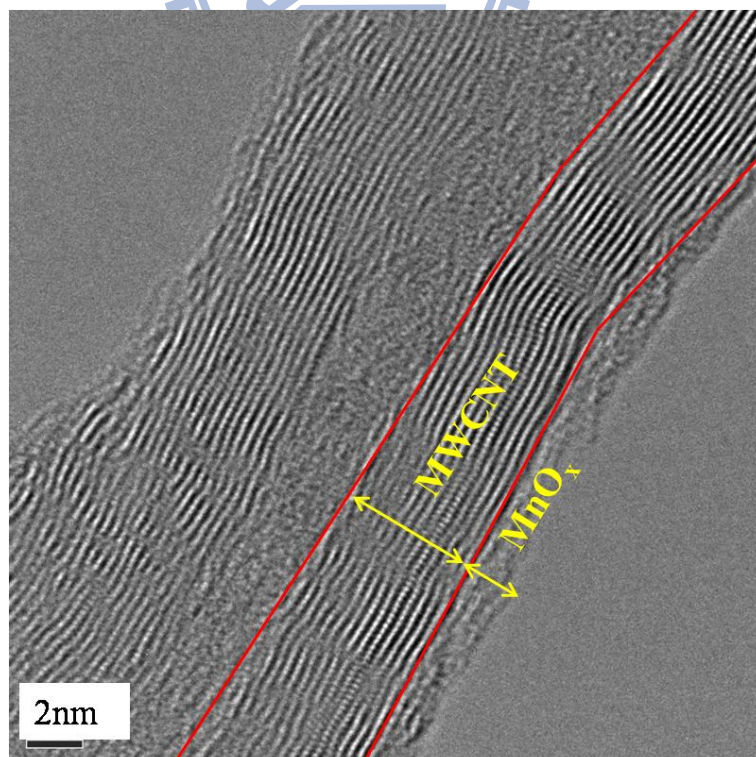


Fig.3-26 TEM image of 30V-20mins after 6000 cycles without thermal annealing

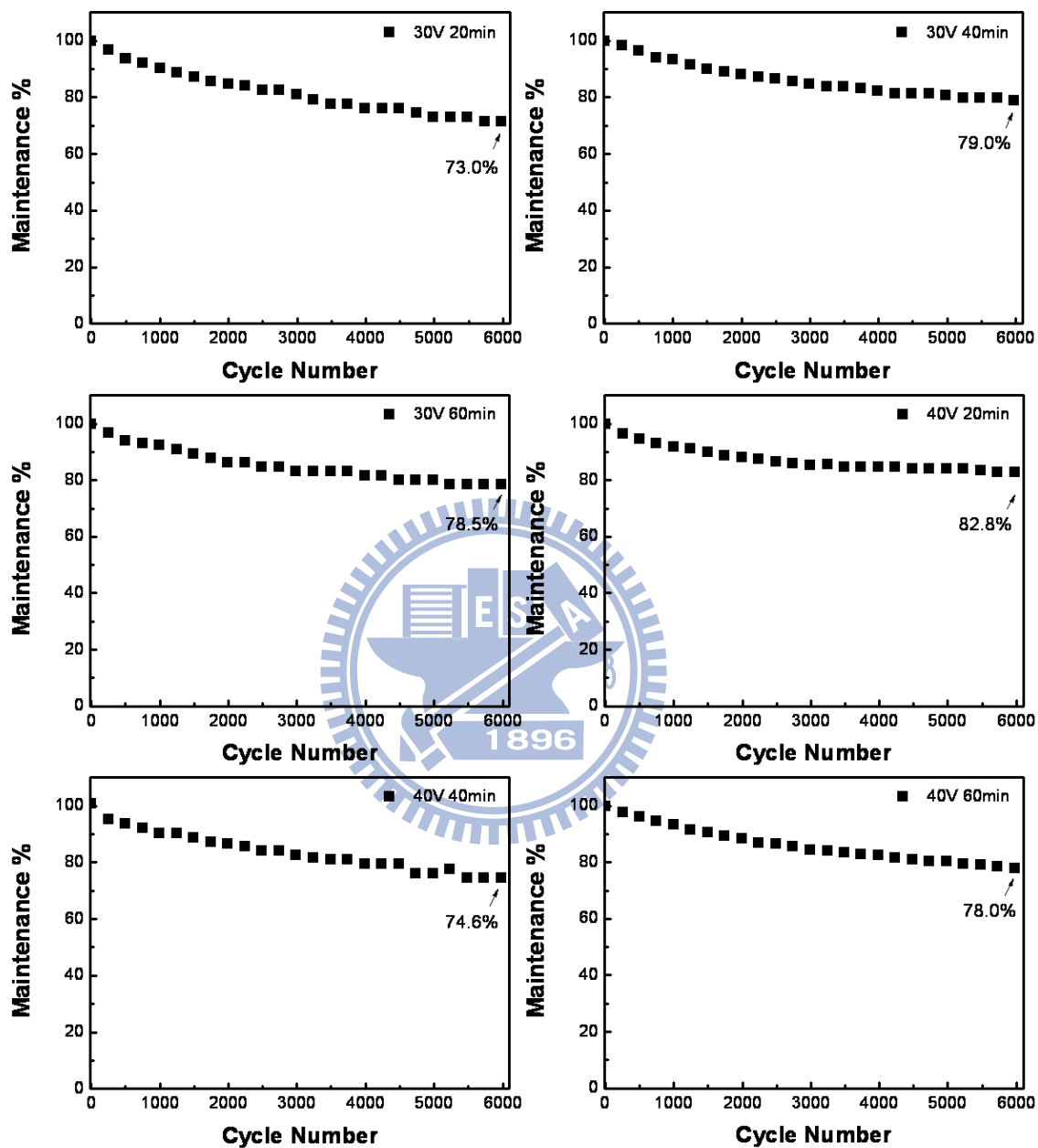


Fig.3-27 1mA constant current stability test of MnO_x/CNT composite electrodes without thermal annealing

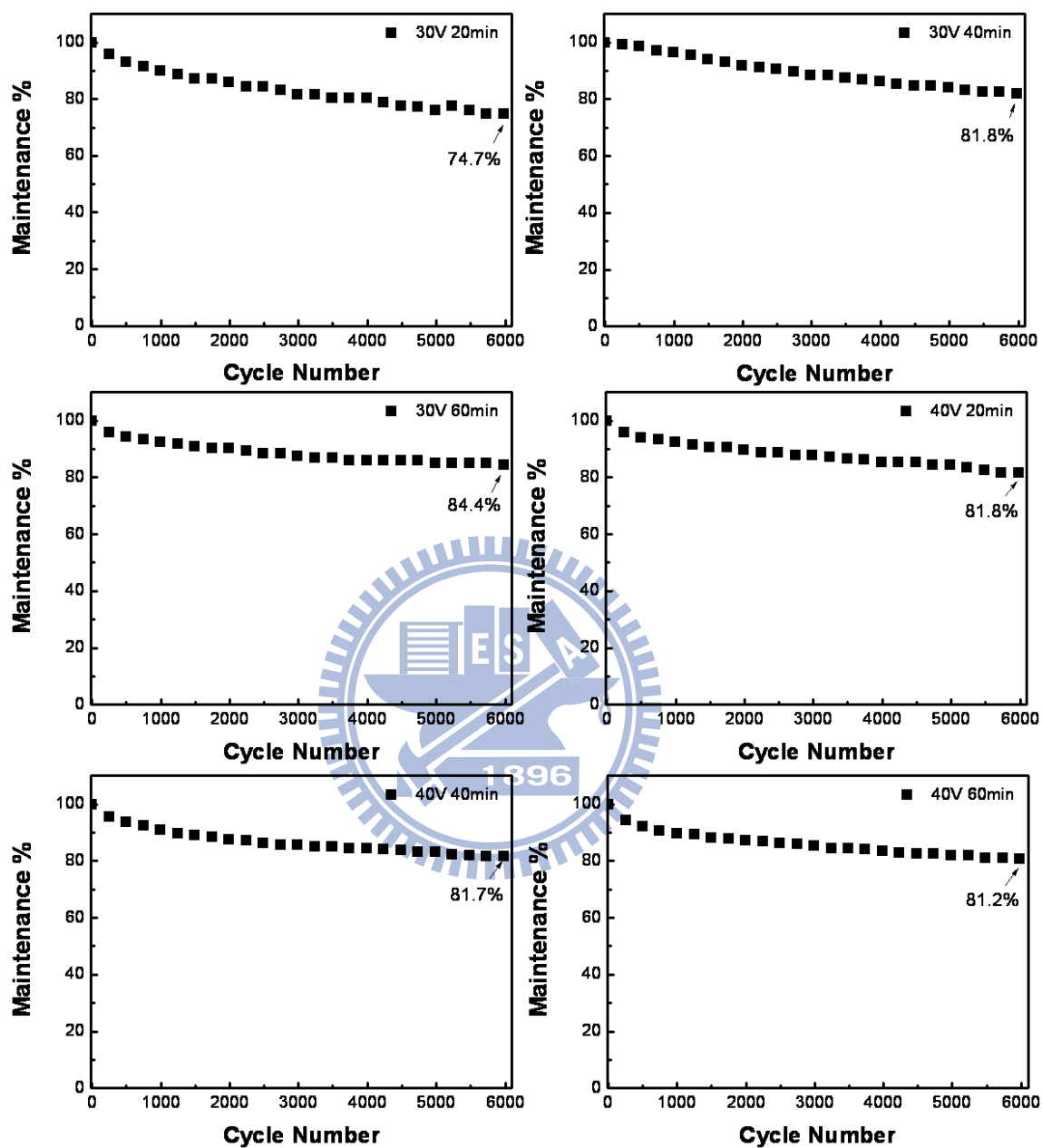


Fig.3-28 1mA constant current stability test of MnO_x/CNT composite electrodes after 150°C for 2 hours

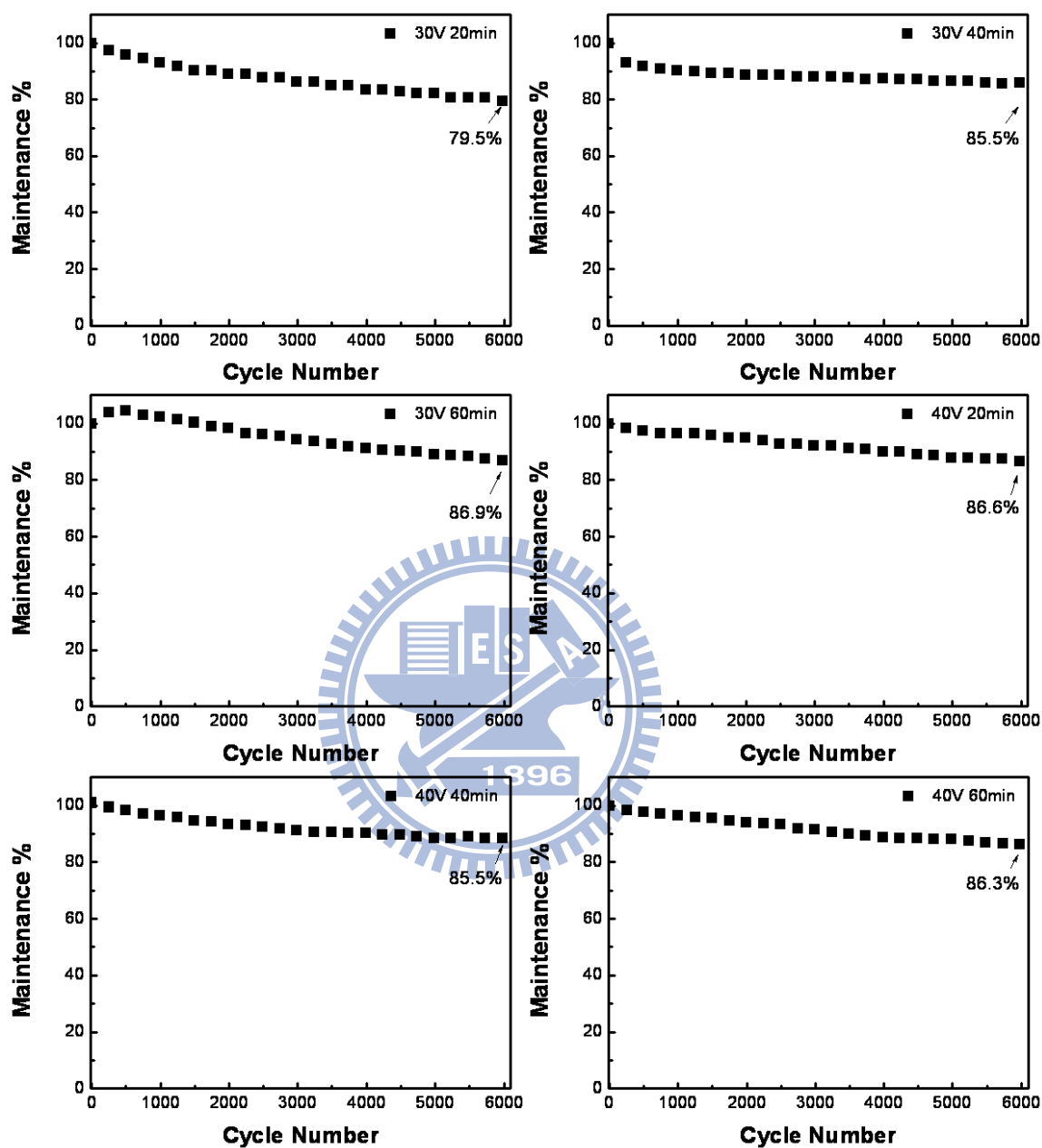


Fig.3-29 1mA constant current stability test of MnO_x/CNT composite electrodes after 200°C for 2 hours

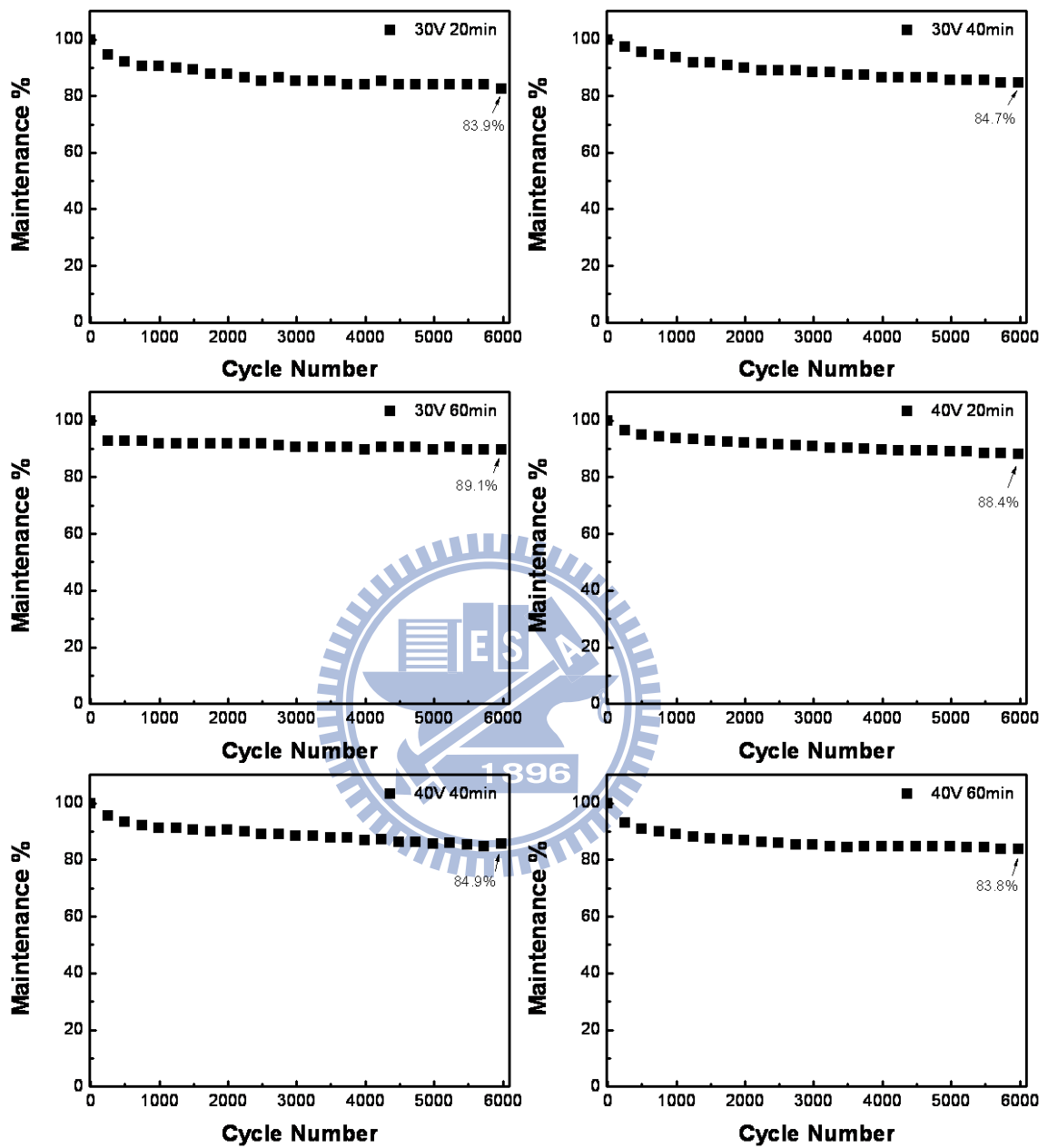


Fig.3-30 1mA constant current stability test of MnO_x/CNT composite electrodes after 250°C for 2 hours

Chapter 4

Conclusions

In this study, we first propose a new technique that substituting hydrogen ion for polymers as surfactant to ionize the surface of manganese oxide to fabricate supercapacitors by electrophoretic deposition method. MnO_x on CNTs/Ni substrate and MnO_x /CNTs composite on Ni remained high specific capacitance at high scanning rate (100mV/s) because the conductivity of MnO_x is improved by CNTs. When cycling, dissolution and peeling of manganese oxide are the main factor in degradation of capacitance. The MnO_x /CNTs composite electrode preserves 79% of its original capacitance in the 6000 cycles of operation which is higher than MnO_x nanopowder supercapacitors due to difference in adhesion of MnO_x .

After annealed the MnO_x /CNTs composite electrodes retain amorphous structure which allows Na^+ ion to fast insert and extract. Therefore the MnO_x /CNTs composite electrodes still have high specific capacitance at 100mV/s, about 80% of it measured at 5mV/s. From XPS analysis, we know that with increasing annealing temperature, the content of MnO_2 is also increased that prefers transforming into MnOOH by which the specific capacitance of composite is enhanced. The specific capacitance can be as high as 846F/g for 40V-20mins after annealed at 200°C for 2 hours. Impedance analysis is also indicating that the charge transfer resistance decreased meaning that the barrier of Na^+ insertion and deinsertion is declined when temperature increased. Stability of composite electrode is also promoted probably due to

better adhesion between manganese oxide and CNTs that reduce the dissolution of MnO_x film. Capacitance can maintain nearly to 80% in overall and the highest can reach 89.1% after 6000 cycles. These electrochemical properties show that combining MnO_x/CNT coaxial composite and ionizing manganese oxide by H^+ ion technique is a useful method to fabricate high specific capacitance, fast reaction rate, and high stability supercapacitors.



References

- 1 R. Kotz and M. Carlen, *Electrochimica Acta* **45**, 2483-2498 (2000).
- 2 B. E. Conway, *Journal of the Electrochemical Society* **138**, 1539-1548 (1991).
- 3 J. P. Zheng, J. Huang, and T. R. Jow, *Journal of the Electrochemical Society* **144**, 2026-2031 (1997).
- 4 Y. Wu and H. Gao, *Vehicular Technology, IEEE Transactions on* **55**, 1748 - 1755 (2006).
- 5 P. Thounthong, V. Chunkag, P. Sethakul, B. Davat, and M. Hinaje, *Vehicular Technology, IEEE Transactions on* **58**, 3892 - 3904 (2009).
- 6 P. Simon and Y. Gogotsi, *Nature Materials* **7**, 845-854 (2008).
- 7 V. L. Pushparaj, M. M. Shaijumon, A. Kumar, S. Murugesan, L. Ci, R. Vajtai, R. J. Linhardt, O. Nalamasu, and P. M. Ajayan, *Proceedings of the National Academy of Sciences of the United States of America* **104**, 13574-13577 (2007).
- 8 P. Thounthong, S. Rael, and B. Davat, *Energy Conversion, IEEE Transactions on* **24**, 247 - 255 (2009).
- 9 B. Pillay and J. Newman, *Journal of the Electrochemical Society* **143**, 1806-1814 (1996).
- 10 B. V. Tilak, C. G. Rader, and S. K. Rangarajan, *Journal of the Electrochemical Society* **124**, 1891-1892 (1977).

- 11 S. Sarangapani, B. V. Tilak, and C.-P. Chen, *Journal of the Electrochemical Society* **143**, p. 1806-1814 (1996).
- 12 H. Shi, *Electrochimica Acta* **41**, 1633-1693 (1996).
- 13 D. Y. Qu and H. Shi, *Journal of Power Sources* **74**, 99-107 (1998).
- 14 J. H. Chen, W. Z. Li, D. Z. Wang, S. X. Yang, J. G. Wen, and Z. F. Ren, *Carbon* **40**, 1193-1197 (2002).
- 15 E. Frackowiak and F. Beguin, *Carbon* **39**, 937-950 (2001).
- 16 V. D. Patake, S. S. Joshi, C. D. Lokhande, and O. S. Joo, *Materials Chemistry and Physics* **114**, 6-9 (2009).
- 17 N. Nagarajan and I. Zhitomirsky, *Journal of Applied Electrochemistry* **36**, 1399-1405 (2006).
- 18 M. Jayalakshmi and K. Balasubramanian, *International Journal of Electrochemical Science* **4**, 878-886 (2009).
- 19 X. Zhao, C. Johnston, and P. S. Grant, *Journal of Materials Chemistry* **19**, 8755-8760 (2009).
- 20 V. R. Shinde, S. B. Mahadik, T. P. Gujar, and C. D. Lokhande, *Applied Surface Science* **252**, 7487-7492 (2006).
- 21 S. G. Kandalkar, J. L. Gunjekar, and C. D. Lokhande, *Applied Surface Science* **254**, 5540-5544 (2008).

- 22 X. F. Wang, Z. You, and D. B. Ruan, *Chinese Journal of Chemistry* **24**, 1126-1132 (2006).
- 23 J. Y. Lee, K. Liang, K. H. An, and Y. H. Lee, *Synthetic Metals* **150**, 153-157 (2005).
- 24 K. W. Nam, W. S. Yoon, and K. B. Kim, *Electrochimica Acta* **47**, 3201-3209 (2002).
- 25 M. S. Wu and H. H. Hsieh, *Electrochimica Acta* **53**, 3427-3435 (2008).
- 26 I. H. Kim, J. H. Kim, Y. H. Lee, and K. B. Kim, *Journal of the Electrochemical Society* **152**, A2170-A2178 (2005).
- 27 V. D. Patake, C. D. Lokhande, and O. S. Joo, *Applied Surface Science* **255**, 4192-4196 (2009).
- 28 J. W. Long, K. E. Swider, C. I. Merzbacher, and D. R. Rolison, *Langmuir* **15**, 780-785 (1999).
- 29 S. L. Chou, F. Y. Cheng, and J. Chen, *Journal of Power Sources* **162**, 727-734 (2006).
- 30 S. L. Chou, J. Z. Wang, S. Y. Chew, H. K. Liu, and S. X. Dou, *Electrochemistry Communications* **10**, 1724-1727 (2008).
- 31 Z. Fan, J. H. Chen, B. Zhang, B. Liu, X. X. Zhong, and Y. F. Kuang, *Diamond and Related Materials* **17**, 1943-1948 (2008).
- 32 X. Jin, W. Zhou, S. Zhang, and G. Z. Chen, *Small* **3**, 1513-1517 (2007).
- 33 C. Y. Lee, H. M. Tsai, H. J. Chuang, S. Y. Li, P. Lin, and T. Y. Tseng, *Journal of the*

- Electrochemical Society **152**, A716-A720 (2005).
- 34 J. Li and I. Zhitomirsky, Colloids and Surfaces a-Physicochemical and Engineering Aspects **348**, 248-253 (2009).
- 35 J. Li and I. Zhitomirsky, Journal of Materials Processing Technology **209**, 3452-3459 (2009).
- 36 S. B. Ma, K. W. Nam, W. S. Yoon, X. Q. Yang, K. Y. Ahn, K. H. Oh, and K. B. Kim, Journal of Power Sources **178**, 483-489 (2008).
- 37 A. L. M. Reddy, M. M. Shaijumon, S. R. Gowda, and P. M. Ajayan, Nano Letters **9**, 1002-1006 (2009).
- 38 M. Toupin, T. Brousse, and D. Belanger, Chemistry of Materials **16**, 3184-3190 (2004).
- 39 Y. H. Wang and I. Zhitomirsky, Langmuir **25**, 9684-9689 (2009).
- 40 C. J. Xu, B. H. Li, H. D. Du, F. Y. Kang, and Y. Q. Zeng, Journal of Power Sources **180**, 664-670 (2008).
- 41 I. H. Kim, J. H. Kim, B. W. Cho, Y. H. Lee, and K. B. Kim, Journal of the Electrochemical Society **153**, A989-A996 (2006).
- 42 D. Choi, G. E. Blomgren, and P. N. Kumta, Advanced Materials **18**, 1178-+ (2006).
- 43 T. Kudo, Y. Ikeda, T. Watanabe, M. Hibino, M. Miyayama, H. Abe, and K. Kajita, Solid State Ionics **152**, 833-841 (2002).

- 44 E. Raymundo-Pinero, V. Khomenko, E. Frackowiak, and F. Beguin, *Journal of the Electrochemical Society* **152**, A229-A235 (2005).
- 45 Y. Q. Wang, A. B. Yuan, and X. L. Wang, *Journal of Solid State Electrochemistry* **12**, 1101-1107 (2008).
- 46 C. Y. Wan, K. Azumi, and H. Konno, *Electrochimica Acta* **52**, 3061-3066 (2007).
- 47 C. J. Xu, B. H. Li, H. D. Du, F. Y. Kang, and Y. Q. Zeng, *Journal of Power Sources* **184**, 691-694 (2008).
- 48 F. Hashemzadeh, M. M. K. Motlagh, and A. Maghsoudipour, *Journal of Sol-Gel Science and Technology* **51**, 169-174 (2009).
- 49 P. Sarkar and P. S. Nicholson, *Journal of the American Ceramic Society* **79**, 1987 - 2002 (1996).
- 50 X. L. Wang, A. B. Yuan, and Y. Q. Wang, *Journal of Power Sources* **172**, 1007-1011 (2007).
- 51 K. W. Nam, C. W. Lee, X. Q. Yang, B. W. Cho, W. S. Yoon, and K. B. Kim, *Journal of Power Sources* **188**, 323-331 (2009).
- 52 V. Subramanian, H. W. Zhu, and B. Q. Wei, *Electrochemistry Communications* **8**, 827-832 (2006).
- 53 C. M. Brett and A. M. O. Breet, Oxford, New York, 405 (1993).
- 54 S. Srinivasana, E. A. Ticianellia, C. R. Derouina, and A. Redondoa, *Journal of Power*

Sources **22**, 359-375 (1988).

55 A. R. Boccaccini, J. Cho, J. A. Roether, B. J. C. Thomas, E. J. Minay, and M. S. P. Shaffer, Carbon **44**, 3149-3160 (2006).

56 W. F. Wei, X. W. Cui, W. X. Chen, and D. G. Ivey, Journal of Power Sources **186**, 543-550 (2009).

57 W. F. Wei, X. W. Cui, W. X. Chen, and D. G. Ivey, Electrochimica Acta **54**, 2271-2275 (2009).

58 C. H. Liang and C. S. Hwang, Japanese Journal of Applied Physics **47**, 1662-1666 (2008).

